A Review on Piezoelectric Energy Harvesting: Materials, Methods, and Circuits

Shashank Priya*, Hyun-Cheol Song, Yuan Zhou, Ronnie Varghese, Anuj Chopra, Sang-Gook Kim, Isaku Kanno, Liao Wu, Dong Sam Ha, Jungho Ryu and Ronald G. Polcawich

A Review on Piezoelectric Energy Harvesting: Materials, Methods, and Circuits

DOI 10.1515/ehs-2016-0028

Abstract: Piezoelectric microelectromechanical systems (PiezoMEMS) are attractive for developing next generation self-powered microsystems. PiezoMEMS promises to eliminate the costly assembly for microsensors/microsystems and provide various mechanisms for recharging the batteries, thereby, moving us closer towards batteryless wireless sensors systems and networks. In order to achieve practical implementation of this technology, a fully assembled energy harvester on the order of a quarter size dollar coin (diameter = 24.26 mm, thickness = 1.75 mm) should be able to generate about 100 μW continuous power from low frequency ambient vibrations (below 100 Hz). This paper reviews the state-of-the-art in microscale piezoelectric energy harvesting, summarizing key metrics such as power density and bandwidth of reported structures at low frequency input. This paper also describes the recent advancements in piezoelectric materials and resonator structures. Epitaxial growth and grain texturing of piezoelectric materials is being developed to achieve much higher energy conversion efficiency. For embedded medical systems, lead-free piezoelectric thin films are being developed and MEMS processes for these new classes of materials are being investigated. Nonlinear resonating beams for wide bandwidth resonance are also reviewed as they would enable wide bandwidth and low frequency operation of energy harvesters. Particle/granule spray deposition techniques such as aerosol-deposition (AD) and granule spray in vacuum (GSV) are being matured to realize the meso-scale structures in a rapid manner. Another important element of an energy harvester is a power management circuit, which should maximize the net energy harvested. Towards this objective, it is essential for the power management circuit of a small-scale energy harvester to dissipate minimal power, and thus it requires special circuit design techniques and a simple maximum power point tracking scheme. Overall, the progress made by the research and industrial community has brought the energy harvesting technology closer to the practical applications in near future.

Keywords: energy harvesting, piezoelectric, MEMS, PiezoMEMS, electromechanical coupling, power density, epitaxial PZT, grain texturing, lead-free, non-linear resonance, aerosol deposition (AD)/granule spray in vacuum (GSV), cantilever, maximum power point

***Corresponding author: Shashank Priya,** Center for Energy Harvesting Materials and Systems (CEHMS), Virginia Tech, Blacksburg, VA 24061, USA, E-mail: spriya@vt.edu
Hyun-Cheol Song: E-mail: songhc@vt.edu, **Yuan Zhou:** E-mail: yzhou6@vt.edu, **Ronnie Varghese:** E-mail: ronniev@vt.edu, **Anuj Chopra:** E-mail: anujchopraiitm@gmail.com, Center for Energy Harvesting Materials and Systems (CEHMS), Virginia Tech, Blacksburg, VA 24061, USA
Sang-Gook Kim, Department of Mechanical Engineering, Massachusetts Institute of Technology, Cambridge, MA 02139, USA, E-mail: sangkim@mit.edu
Isaku Kanno, Department of Mechanical Engineering, Kobe University, Kobe 657–8501, Japan, E-mail: kanno@mech.kobe-u.ac.jp
Liao Wu, Dong Sam Ha: E-mail: ha@vt.edu, Department of Electrical and Computer Engineering, Virginia Tech, Blacksburg, VA 24061, USA
Jungho Ryu, Functional Ceramics Group, Korea Institute of Materials Science (KIMS), Changwon, Gyeongnam 51508, Korea, E-mail: jhryu@kims.re.kr
Ronald G. Polcawich, US Army Research Laboratory, Adelphi, MD 20783, USA, E-mail: ronald.g.polcawich.civ@mail.mil

1 Introduction

The vast reduction in the size and power consumption of sensors and CMOS circuitry has led to a focused research effort on on-board power sources which can replace or recharge batteries. The concern with batteries has been that they must be charged before use. Similarly, the sensors and data acquisition components in distributed networks require centralized energy sources for their operation. In some applications such as sensors for structural health monitoring in remote locations, geographically inaccessible temperature or humidity sensors, battery charging or replacement operations can be costly or even impractical. The need to replace batteries in a large-scale sensor network can be problematic and costly. The replacement is nearly impossible in hazardous, harsh and large terrain deployment. An example would be embedded sensor networks in urban battlefields. Logically, the emphasis in such cases has been on developing the on-site generators that can transform any

available form of energy at that location into electrical energy (Priya and Inman 2009). Recent advances in low-power VLSI design have enabled ultra-small power integrated circuits, which can run with only 10's nW to 100's μW of power (Chandrakasan et al. 1998). This scaling trend has opened the door for on-chip energy harvesting solutions, eliminating the need for chemical batteries or complex wiring for micro-sensors and thus forming the foundation for battery-less autonomous sensors and network systems.

An alternative to implementation of a conventional battery as power supply is to make use of the parasitic energy available locally in the environment. Unused energy is produced by industrial machines, human activity, vehicles, structures and environment sources, all of which could be an excellent source of capturing small power without affecting the source itself. Furthermore, the energy harvesting can provide solution for harsh environmental conditions unfit for battery use for example for temperature exceeding 60 °C. In recent years, several energy harvesting approaches have been proposed using solar, thermoelectric, electromagnetic, piezoelectric, and capacitive schemes at meso, micro and nano scales (Beeby, Tudor, and White 2006; Priya and Inman 2009; Wang and Song 2006). These can be simply classified in two categories: (i) energy harvesting for sensor and communication networks using Microelectromechanical systems (MEMS)/thin film approach, and (ii) energy harvesting for electronic devices using bulk devices. MEMS devices combine the response of electrical and mechanical components. The size of these devices varies from sub-micron to millimeter range. MEMS integration with modern electronics provides, capability to interact with vast range of platform leading to new and enhanced functionality for sensors and energy harvesters.

Mechanical vibration energy can be converted into electrical energy using piezoelectric, electromagnetic and electrostatic transducers. Out of them, piezoelectric transducers are considered more attractive option due to their high energy density (Roundy and Wright 2004). In comparison to the electrostatic transducers, piezoelectric MEMS devices offer following advantages: (1) scaling of devices for miniaturization because the energy density of piezoelectric materials remains high with reducing film thickness, (2) low voltage operation of piezoelectric actuators, (3) additional possibility to harvest energy due to coupling between mechanical and electrical component, and (4) easy implementation of high frequency, and temperature-stable resonant devices. Since thin films of piezoelectric materials provide the possibility to design more economical and thinner size devices, a lot of research on fabrication of piezoelectric thin films for MEMS devices has been conducted.

This paper mainly focuses on small-scale power energy harvesting techniques (~ 1–100 μW) using a MEMS/thin film/thick film approach for the self-supported operation of portable or embedded micro devices and systems. Further, we focus on mechanical vibration energy as the prime source for generating electric power. The question one might ask at this stage is: "What is the best mechanism for converting mechanical energy into electrical energy at the ~mm^3 dimensions?" Priya et al. have studied the scaling of output power as a function of effective material volume (V) for different mechanisms (Marin, Bressers, and Priya 2011). By taking into account constitutive equations for the respective conversion mechanism, the output power of electromagnetic mechanism is proportional to V^2, while that of piezoelectric mechanism is proportional to $V^{\frac{3}{4}}$. Thus, at smaller scales, the piezoelectric mechanism becomes more attractive as compared to electromagnetics. To obtain an approximation of the critical size where piezoelectricity becomes more useful, Figure 1 plots harvester volume vs. normalized output power (normalized by acceleration and multiplied by frequency) for various piezoelectric and electromagnetic prototypes reported in the literature (Marin, Bressers, and Priya 2011). From Figure 1, it can be determined that ~0.5 cm^3 is in the vicinity of the critical size. At a smaller device volume than this critical size, the electromagnetic transformation factor (similar to electromechanical coupling in piezoelectrics) $\Phi_T \cong \sum B(y_c, z_c)(\Delta L_{coil}) \cos(\theta(y_c, z_c))\Phi(y_b)$

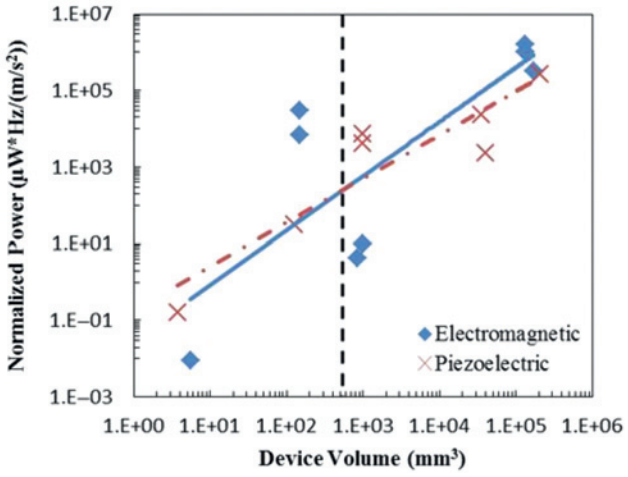

Figure 1: Output power as a function of effective material volume for piezoelectric and electromagnetic vibration energy harvesting mechanisms. Variation of output power normalized by acceleration and multiplied by frequency as a function of device volume for various energy harvesters found in literature and commercially (Marin 2013).

reduces sharply with decrease in magnitude of induction and length of coil. Here B represents the magnetic field, L is the length of coil, θ is the angle between $\vec{z} \times \vec{B}$ and the differential conductor length $\vec{dl}$, y_c, z_c are coordinates on plane of the coil, and y_b is the coordinate on the beam. Another major problem with inductive harvesters at small scales is their low output voltage, which makes it difficult to use rectification and AC/DC conversion circuits (Bono et al. 2009). In addition to the normalized power and output voltage, assembly at this scale critically affects the cost of the system. Below the critical volume, assembly of the conductive induction coil and magnetic layer becomes challenging. The mechanisms at this scale can be cost-effective if they can be fabricated by monolithic MEMS processes without substantial post assembly efforts. Thus for MEMS-scale energy harvesters smaller than ~0.5 cm^3, piezoelectric transduction is the most appropriate scenario. Electrostatic harvesters have the surface potential decay problem because dielectrics are not perfect insulators. Specially, the surface potential decay is severe in an extremely moist environment since most surplus charges on or just below the surface of electret materials are neutralized by the ions in the water. (Sessler 2001; Sorimachi, Takahashi, and Tokonami 2009). We should point out that the use of synchronous circuits has been shown to be a viable alternative for such systems (Lefeuvre et al. 2014). On the other hand, piezoelectric harvester can directly convert mechanical energy into electric energy and can be directly integrated into monolithic MEMS-scale systems (Beeby, Tudor, and White 2006; Hajati and Kim 2011; Jeon et al. 2005; Kang et al. 2016; Kim et al. 2009; Morimoto et al. 2010; Muralt, Polcawich, and Trolier-McKinstry 2009b; Roundy and Wright 2004).

There is commonly a concern whether one can one achieve self-powering when the power required is much larger than that can be achieved by MEMS-scale piezoelectric harvester. Most reported piezoelectric devices show orders of magnitude smaller normalized power density than that required by the sensors and systems at the present time. In scenarios where multiple environmental resources are available besides mechanical energy, self-powering may be achieved by developing a smart architecture, which utilizes all the environmental resources such as, wind, magnetic fields, light, sound, temperature gradients, and RF waves. However, the best scenario for cost and size is to improve the MEMS-scale piezoelectric harvester technology to generate enough power. The physics behind the piezoelectrically generated power is reviewed in this paper along with approaches to enhance the power density by addressing piezoelectric materials, magneto-electrics and non-linear structural designs. Further discussion on common energy harvesting circuit topology is provided that can boost the transfer of harvested energy into storage devices.

The general principle for conversion of low frequency mechanical stress into electrical energy using a piezoelectric transducer is shown schematically in Figure 2 (Kim et al. 2007). This transformation from mechanical to electrical energy is obtained through the direct piezoelectric effect. The resulting energy can be stored after using a rectifier and DC-DC converter circuit. There are three primary steps in power generation as outlined in this schematic: (a) trapping the mechanical AC stress from available source, (b) converting the mechanical energy into electrical energy by direct piezoelectric transduction, and (c) processing and storing the generated electrical energy. Depending upon the frequency and amplitude of the mechanical stress, one can design the required transducer, its dimensions, vibration mode and the desired piezoelectric material. The power density of a harvesting system is dependent upon the strategies that

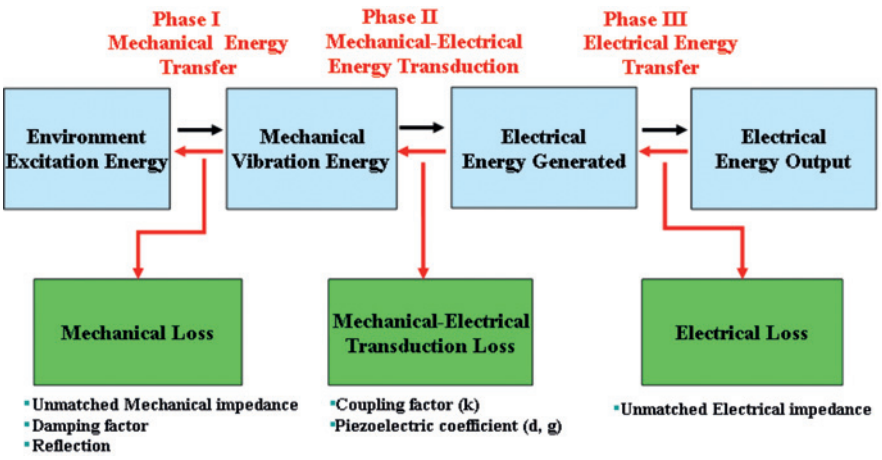

Figure 2: Energy flow of a piezoelectric generator (Kim et al. 2007).

maximize the trapping of energy and reduce the losses occurring at each step, namely, mechanical loss due to mismatch in mechanical impedance, and electromechanical loss depending upon the magnitude of the coupling factor (Findeisen 2013; Ginsberg and Ginsberg 2001; Jiang and Miles 1999; Uchino 2009).

Most reported piezoelectric harvesters utilize the resonance of a cantilever beam structure, which amplifies the small ambient vibration into an in-plane strain governed by the Euler – Bernoulli beam equation (Beeby, Tudor, and White 2006; Muralt, Polcawich, and Trolier-McKinstry 2009b; Priya and Inman 2009). In order to harvest power robustly, the bandwidth of a linear cantilever beam harvester should be wide enough to accommodate the uncertain variance of ambient vibrations (Hajati and Kim 2011). Therefore, the resonance bandwidth is an important characteristic for trapping sufficient amount of energy to the beam and should be accounted for determining the performance of energy harvesters. Piezoelectric MEMS technology is the most cost-effective energy harvesting technology if it can provide high enough power density and wide enough bandwidth. Three major attributes to make the piezoelectric MEMS energy harvesting technology deployable for real applications are: the cost of the system, the normalized power density and the operational frequency range (bandwidth and the center frequency). The current state-of-the-art piezoelectric MEMS technologies are reviewed in this paper with respect to these attributes.

2 Review of Piezoelectric Energy Harvesting

The basic principle of piezoelectric cantilever based energy harvester can be explained by accounting for the flow of energy between different domains in Phase I and Phase II as shown in Figure 2. Ambient vibration injects energy into the system through the base excitation at each cycle. This input energy is converted to kinetic energy of the proof mass and then to potential energy stored as the beam's mechanical strain (Hajati 2011). Part of the elastic energy stored in the beam is transformed into electrical energy in the form of induced charge across the piezoelectric layer, which is deposited on the beam. Piezoelectric energy harvesters generally have bimorph or unimorph cantilever beam structures (Figure 3) (Renaud et al. 2008; Roundy and Wright 2004). However, at the MEMS-scale, bimorph cantilever are less manufacturable with existing microfabrication processes. As a result, MEMS cantilevers mostly have a unimorph configuration. A seismic mass is usually attached at the tip of the cantilever to adjust the resonant frequency to the available environmental frequency, normally below 100 Hz (Reilly et al. 2009; Roundy, Wright, and Rabaey 2003).

Recently, MEMS technologies have been applied towards the development of integrated energy harvesters, and many piezoelectric MEMS energy harvesters have been developed (Aktakka 2012; Beeby, Tudor, and White 2006; Bertacchini et al. 2011; Defosseux et al. 2012; Durou et al. 2010; Elfrink et al. 2009a, 2009b, 2010; Erturk and Inman 2008; Fang et al. 2006; Hajati and Kim 2011; Hirasawa et al. 2010; Isarakorn et al. 2011; Jeon et al. 2005; Lee et al. 2009; Lei et al. 2011; Marzencki et al. 2007; Massaro et al. 2011; Miller et al. 2011; Muralt et al. 2009a; Park, Park, and Lee 2010; Roundy, Wright, and Rabaey 2003a, 2003b; Shen et al. 2008; Van Schaijk et al. 2008; Xu et al. 2012b; Yen et al. 2011). Useful metrics in comparing these devices are their active area, active volume, resonant frequency, harvested power and power densities in volume or area. Devices with relatively higher power densities (in volume or area) or non-PZT materials such as AlN and lead-free KNN are selectively shown in Table 1. In order to understand the performance attributes defined earlier and better compare the devices reported, basic models of vibration kinematics and piezoelectrics are summarized below.

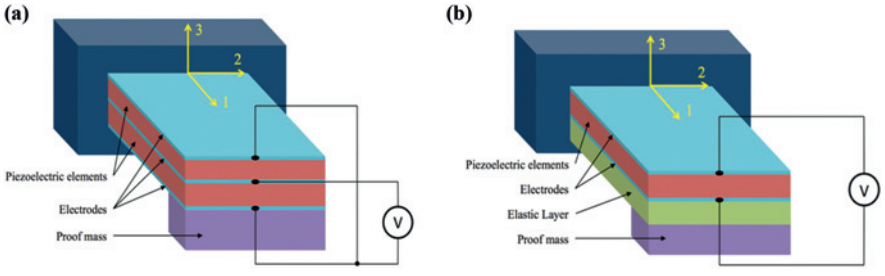

Figure 3: Basic structure of piezoelectric energy harvesters: (a) Bimorph structure, (b) Unimorph structure.

Table 1: Comparison of recent small scale piezoelectric energy harvesters.

Reference	Active material	Active area, mm^2	Active volume, mm^3	Acceleration, g	Frequency, Hz	Power, μW	Normalized areal power density, ($\mu W/(mm^2.Hz.g^2)$)	Normalized Volumetric power density, ($\mu W/(mm^3.Hz.g^2)$)
Muralt et al. (2009a)	PZT, d_{33}	0.96	0.48	2.0	870	1.4	4.19×10^{-4}	8.38×10^{-4}
Morimotoet et al. (2010)	PZT, d_{31}	76.5	4.05	0.5	126	5.3	2.20×10^{-3}	4.15×10^{-2}
Hajati and Kim (2011)	PZT, d_{33}	120	0.02	4.0	1300	22	8.81×10^{-6}	5.29×10^{-2}
Durou et al. (2010)	PZT		464	0.2	76	13.9		9.85×10^{-3}
Defosseux et al. (2012)	AlN, d_{31}	3.573 (est.)	2.8	0.275	214	0.63	1.09×10^{-2}	1.39×10^{-2}
Marzencki et al. (2007)	AlN, d_{31} (vac.)	1.573 (est.)	–	0.126	214	0.55	1.03×10^{-1}	
Hirasawa et al. (2010)	AlN		1.63	1.0	857	0.18		1.29×10^{-4}
Elfrink et al. (2010)	AlN		15	0.2	599	69		1.92×10^{-1}
Xu et al. (2011a)	PZT		20.9	1.0	329	7.35		1.07×10^{-3}
Lei et al. (2011)	PZT		18.6	1.0	235	14		3.20×10^{-3}
Park, Park, and Lee (2010)	PZT, d_{33}	1.8	1.05	0.39	528	1.1	7.61×10^{-3}	1.30×10^{-2}
Fang et al. (2006)	PZT, d_{31}	2.65	0.78	1.0	608	2.16	1.34×10^{-3}	4.55×10^{-3}
Lee et al. (2009)	PZT, d_{31}	4.5	0.452	2.5	255.9	2.765	3.84×10^{-4}	3.82×10^{-3}
Aktakka (2012)	PZT, d_{31}	49	27	1.5	154	205	1.21×10^{-2}	2.19×10^{-2}
Kanno et al. (2012)	KNN, d_{31}	56.1	11.4	1.0	1036	1.1	1.89×10^{-5}	9.31×10^{-5}

Source: Initial data was taken from Park, Park, and Lee (2010) and Aktakka (2012) and updated to reflect the new developments. Devices with high power density (in volume or area) or typical non-PZT devices are selected.

2.1 Fundamentals of Piezoelectricity

Piezoelectricity is the property of certain crystals to generate an electric potential in response to applied mechanical stress. There are two different kinds of phenomena commonly observed which are termed as direct and the converse piezoelectric effects. When the mechanical stress is applied to a piezoelectric material, an electric charge proportional to the applied stress is produced. This refers to the direct piezoelectric effect. Conversely, when electric field is applied to the same material, strain or displacement is produced proportional to the magnitude of electric field. This is called as converse piezoelectric effect. The following two constitutive equations are used to describe the piezoelectric effect:

$$D_i = d_{ij}\sigma_j + \varepsilon_{ii}^T E_i \quad \text{or} \quad D_i = e_{ij}S_j + \varepsilon_{ii}^S E_i \qquad [1]$$

$$S_j = s_{ij}^E \sigma_j + d_{ij}E_i \quad \text{or} \quad \mathrm{T_j = c_{ij}^E S_j - e_{ij}E_i} \qquad [2]$$

Here in these two constitutive equations, D_i is the electrical displacement, S_j is mechanical strain, σ_j is mechanical stress, E_i is the electric field, c_{ij} is the elastic stiffness coefficient, s_{ij} is the elastic compliance coefficient, and ε_{ij} is the permittivity. The superscript used in the equation shows the constant parameter used. d_{ij} and e_{ij} are piezoelectric coefficients which are third rank tensors.

Piezoelectric ceramics are anisotropic in nature implying that the electromechanical properties exhibit maximum along specific crystallographic direction. The properties are commonly described using two subscripts (reduced order tensor notation) which indicate the direction of the electrical and mechanical parameters. Figure 4 shows the direction indexes of constants in rectangular crystallographic system. The principal properties along X, Y and Z axes are described using 1, 2 and 3 notations, respectively. The shear constants are represented by 4, 5 and 6 respectively. For example, in case of piezoelectric charge constant d_{31}, the first index "*3*" indicates that electrodes are perpendicular to axis 3 and the second index "*1*" indicates that the applied stress or induced strain is along direction 1. A superscript index on the electromechanical constant is used to represent the constant condition under which measurements were conducted. For example – in case of compliance, s_{36}^E, "*E*" indicates that the compliance was measured under constant electric field or with electrodes connected together.

Non-centrosymmetricity is requirement for observing the piezoelectric effect and most of the high performance piezoelectric materials are ferroelectric perovskites as shown in Figure 5. The leading representative of the perovskite piezoelectric ceramics, $Pb(Zr,Ti)O_3$ (PZT), has many possible variations depending upon the doping and solid solution. As shown in Figure 4(a), PZT unit cell has

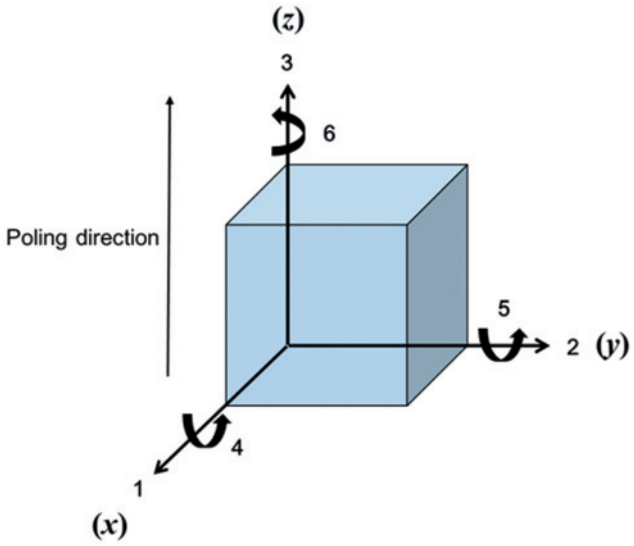

Figure 4: Direction index of electromechanical constants in poled piezoelectric ceramics.

a symmetric cubic structure above the Curie temperature (paraelectric), however, below that it transforms into asymmetric tetragonal structure (approximately Zr/Ti ratio <1, where Zr + Ti = 1) as schematically depicted in Figure 5(b). Thus, PZT unit cell shows spontaneous polarization because of the shift in the position of B-site atom.

Neighboring dipoles formed in the distorted perovskite unit cell align together to form domains. Typically, polycrystalline piezoelectric ceramics have randomly oriented domain distribution as shown in Figure 6(a), thus, overall net polarization of material is negligible. Because of the ferroelectric nature of the material, domains can be permanently aligned by applying strong electric field. This process is called poling (see Figure 6(b)) and is normally performed at an elevated temperature slightly below Curie point to facilitate the domain wall motion. During poling process, most of the domains are aligned along applied electric field direction and neighboring domains exhibit new dimensions through nucleation and growth. After poling process, most of the dipoles retain their alignment imparting the piezoelectric material a remanent polarization (see Figure 6(c)).

Besides piezoelectric ceramics, there are piezoelectric polymer materials which have semi-crystalline structure for examples polyvinylidene fluoride (PVDF), polyamides, ParyleneC, liquid crystal polymers, PVDF-TrFE block copolymer etc. The operation principle of these piezoelectric polymers are similar to piezoelectric ceramic

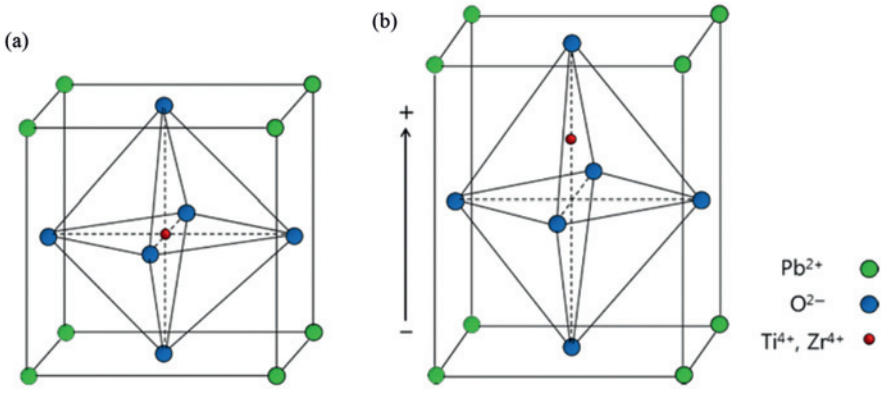

Figure 5: Perovskite PZT unit cell. (a) PZT unit cell in the symmetric cubic state above the Curie temperature. (b) Tetragonally distorted unit cell below the Curie temperature.

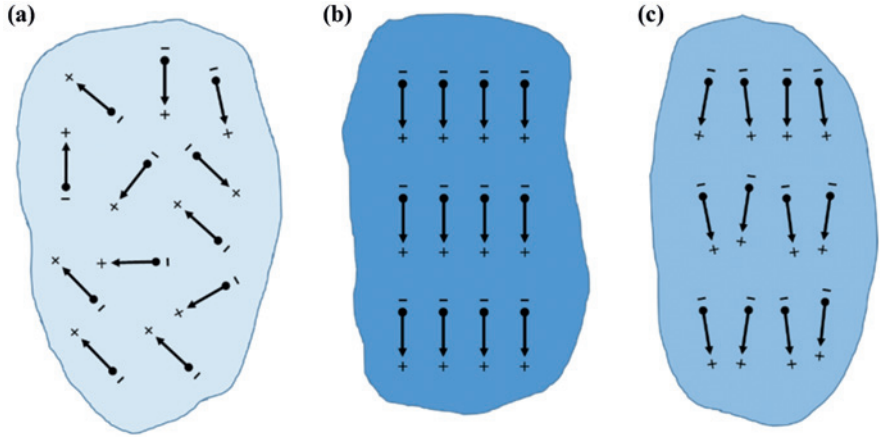

Figure 6: Piezoelectric domains in piezoelectric materials. (a) Randomly oriented domains, (b) Domains during and (c) after poling process.

materials. The semi-crystalline polymers have microscopic crystals inside matrix which are also polarized and function as dipoles as described Figure 6. The microcrystals are distributed within an amorphous matrix. To obtain effective piezoelectricity in such materials, these small crystals should be reoriented and kept in one orientation through electrical poling or mechanical stretch process. There is another type of piezoelectric material known as voided charged polymer (VCP, sometimes called ferroelectret or piezoelectret) that contains internal gas voids. When the polymer surfaces surrounding the void are charged by electrical poling or X-ray, the space charges are created inside matrix and the VCP behaves like piezoelectric material. These polymers have very high d_{33} values. However, these piezoelectric polymers have serious life time and ageing problems. The VCP is easily neutralized in extremely moist environment and the surface charge can be rapidly decayed in high temperature.

2.2 Transfer Function for Energy Harvester

The simple vibration energy harvester can be modeled as a second-order, spring-mass system. The characteristics of the energy harvester can be described by damping constant and natural frequency of the system. A cantilever beam structure with piezoelectric plate and proof mass is equivalent to a lumped spring mass system of a vibrating rigid body. Thus, the governing equation of motion of a lumped spring mass system can be written as:

$$m \cdot \frac{d^2z(t)}{dt^2} + b \cdot \frac{dz(t)}{dt} + k \cdot z(t) = -m \cdot \frac{d^2y(t)}{dt^2} \quad [3]$$

which can be transformed using Laplace transform as following:

$$m \cdot s^2 z(s) + b \cdot s \cdot z(s) + k \cdot s \cdot z(s) = -m \cdot a(s) \quad [4]$$

where $a(s)$ is the Laplace transform of the acceleration, $a(t)$, given as:

$$a(t) = \frac{d^2y(t)}{dt^2} \quad [5]$$

Therefore, the transfer function of the energy harvester can be expressed as:

$$\frac{z(s)}{a(s)} = \frac{1}{\left(s^2 + \frac{b}{m}s + \frac{k}{m}\right)} = \frac{1}{(s2 + \omega r\ Qs + \omega r2\ )} \quad [6]$$

where $Q = \sqrt{km}/b$ is quality factor of system and ω_r is resonance frequency of the energy harvester. The natural frequency of the spring mass system and energy harvester can be given as:

$$\omega_n = \sqrt{\frac{K}{M}} \quad [7]$$

where K and M are the transverse stiffness and effective mass, respectively. The stiffness K can be calculated from loading condition. In case of simple cantilever beam structure, the stiffness can be expressed as:

$$K = 3EI/L^3 \quad [8]$$

where E is modulus of elasticity, I is the moment of inertia, and L is the length of beam. The moment of inertia for a rectangular cross-section is $I = \left(\frac{1}{12}\right)bh^3$, where b and h are the width and thickness of the beam in transverse direction, respectively.

2.3 Frequency Dependence of Output Power

The vibration displacement of energy harvester can be maximized in resonance. The harvester will convert mechanical to electric energy most effectively when the applied vibration frequency is closer to the fixed natural frequency of the device. As shown in Figure 7, a few percent of mismatched frequency with resonance results in a dramatic decrease of output power. Therefore, tuning or adjusting frequency to an external vibration source is essential in order to improve energy conversion efficiency. From eq. [7], the natural

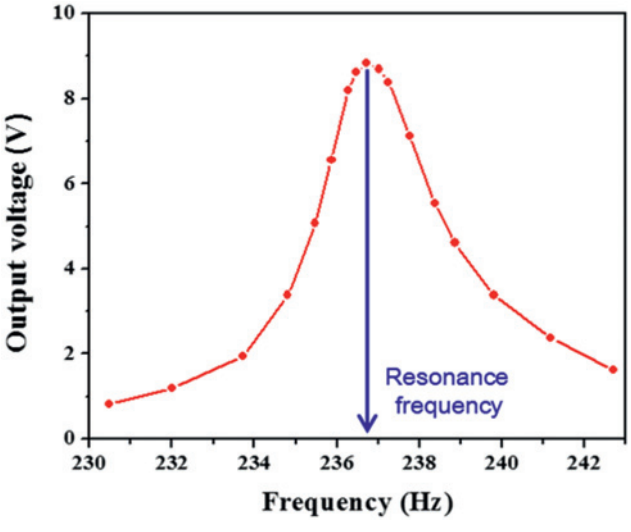

Figure 7: Frequency dependent output power of typical vibration energy harvester. The maximum output power can be achieved at resonance frequency.

frequency of the energy harvester is closely related to dimension and effective mass. The natural frequency of the energy harvester is usually adjusted by changing the weight of proof mass. However, the bandwidth at resonance frequency is usually narrow and thus needs some additional mechanism to effectively capture ambient vibrations which usually represent a wide spectrum of frequencies or time varying vibration spectra.

2.4 Vibration Kinematics

Vibration is common ambient energy source that can be found in household appliances (refrigerators, microwave ovens, washing machines etc.), large civil structures (buildings, bridges etc.), industrial plant (refineries), automobiles and many other common locations. Table 2 shows some of the common sources of mechanical energy that can be harnessed through piezoelectrics. Table 3 quantifies the vibration energy available in some of these environments (Marin and Priya 2012; Priya 2007).

The general model of a vibration energy harvester is a typical mass-spring-damper system. Maximum power is achieved when the excitation frequency ω is equal to the natural frequency ω_n. Maximum extractable electrical power in terms of mechanical damping ratio ζ_m, electrical damping ratio ζ_e, proof mass m and acceleration A becomes,

$$P = \frac{\zeta_e}{4\omega_n(\zeta_e + \zeta_m)^2} mA^2 \quad [9]$$

Several conclusions can be drawn from the observation of eq. [9] (Xu 2012). The extractable power from the beam is inversely proportional to resonance frequency at a fixed acceleration, A; therefore the energy harvester should be designed at lowest possible frequency to achieve highest power if we do not consider that frequencies of external vibration sources are normally fixed in real applications. The extractable power is also proportional to the square of acceleration (Chandrakasan et al. 1998), which limits the energy available for conversion with low-g vibrations whatever the specific design is chosen. It can also be seen that power is proportional to the proof mass, so a large proof mass is always desirable for energy harvesting. Finally, the term composed of the mechanical and electrical damping ratio implies that the maximum power is achieved when the electrical damping matches the mechanical damping (Dutoit, Wardle, and Kim 2005). When the electrical damping is equal to mechanical damping ($\zeta_e = \zeta_m$), the maximum electrical power is given as:

$$P_{\varepsilon,\,\max}(\omega_n) = \frac{mA^2}{16\omega_n\zeta_m} = \frac{mY^2\omega_n^3}{16\zeta_m} \quad [10]$$

where the acceleration amplitude A and proof mass deflection Y are related by the relationship given as:

Table 2: Sources of energy available in the surrounding which are/can be tapped for generating electricity.

Human body	Vehicles	Structures	Industrial	Environment
Breathing, blood pressure, exhalation, body heat	Aircraft, uav, helicopter, automobiles, trains	Bridges, roads, tunnels, farm house structures	Motors, compressors, chillers, pumps, fans	Wind, solar, temperature gradient, daily temperature
Walking, arm motion, finger motion, jogging, swimming, eating, talking	Tires, tracks, peddles, brakes, shock absorbers, turbines	Control-switch, hvac systems, ducts, cleaners, etc.	Conveyors, cutting g and dicing, vibrating mach.	Ocean currents, acoustic waves, em waves, rf signal

Table 3: Peak acceleration and frequency of common structures (Aktakka 2012; Lee et al. 2009).

Vibration source	Peak acceleration (m/s^2)	Frequency (Hz)
Base of a 5 HP 3-axis machine tool	10	70
Notebook computer while CD is being read	0.6	75
Clothes dryer	3.5	120
Second story floor of a wood frame office building	0.2	100
Railway	1.078–1.568	12–16
Truck	1.96–3.43	8–15
Ship	0.98–2.45	12–13

$$A = \omega_n^2 Y \quad [11]$$

Equation [10] represents the theoretical maximum of extractable power, which can be dissipated in the electrical load. This is actually a limiting factor for all linear resonator based energy harvesters if the piezoelectric layer's transformation capacity is not a limiting factor. It has been reported that a nonlinear resonator based energy harvester can circumvent this limit and is able to generate much higher power than the mechanical damping, which will be discussed in the later section. Another parameter of interest in design of thin film harvesters is given by the generalized electromechanical coupling (GEMC) factor, k_G^2 (Uchino 2009). The GEMC factor is obtained from the equation:

$$k_G^2 = \frac{\omega_{short}^2 - \omega_{open}^2}{\omega_{short}^2} \quad [12]$$

where ω_{short} and ω_{open} are the angular resonance frequencies of the associated short and open circuits, respectively. The GEMC represents the power generation performance of the vibration harvesters, and this value can be theoretically derived from the mechanical properties, thickness ratio, and electromechanical coupling factors of piezoelectric thin films (Wang et al. 1999).

2.5 Energy Conversion and Figures of Merit

Piezoelectric energy harvesters can be categorized by the targeted energy sources, such as ambient vibrations, impact or shock stress, fluid flow and human motion. Regardless of the various energy sources, the basic working principle is the same – the environment applies a stress on piezoelectric material and by the direct piezoelectric effect, the input mechanical energy is converted in to electrical energy. Piezoelectric generators produce high voltages and low currents, and require no voltage source to operate. Some believe they are more difficult to be integrated into microsystems (Roundy, Wright, and Rabaey 2003a), but there have been several successful implementations of MEMS scale piezoelectric energy harvesters (see Table 1). In case of the thin films, piezoelectric response is drastically reduced compared to bulk PZT due to clamping effect of the substrate (Lefki and Dormans 1994; Li et al. 2004). Since both longitudinal and transverse piezoelectric components are coupled to each other, thus on application of electric field normal to the films surface, an expansion in longitudinal piezoelectric response and a contraction in transverse piezoelectric response is observed due to clamping effect. The effective piezoelectric coefficient of a thin film on a rigid substrate can be written as (Bono et al. 2009; Krulevitch et al. 1996).

$$d_{33,f} = d_{33} - 2d_{31}\frac{s_{13,f}}{s_{11,f} + s_{12,f}} \quad [13]$$

$$e_{31,f} = e_{31} - \frac{c_{13}^E}{c_{33}^E} e_{33}^E \quad [14]$$

Since the second term in the right hand side of eq. [13] contributes negatively to the effective piezoelectric response, thus effective piezoelectric response is reduced. The electromechanical coupling coefficient (k) is another parameter which is very important especially in resonating structures. The electromechanical coupling coefficient can be given as:

$$k_{33} = \sqrt{\frac{d_{33}^2}{e_{33}^T s_{33}^E}} \quad [15]$$

The electromechanical coupling coefficient represents the ratio of the mechanical (electrical) energy converted into the input electrical (mechanical) energy for the piezoelectric material.

Two piezoelectric modes, d_{31} or d_{33}, are commonly used in piezoelectric micro devices (Figure 8). The relative directions of the electric field and the strain distinguish them: d_{31} when the electric field is perpendicular to the input strain, d_{33} when they are parallel (Bernstein et al. 1999). Conventional MEMS piezoelectric devices/actuators have d_{31} configuration in which a piezoelectric layer is sandwiched between top and bottom electrodes. For a d_{31} mode energy harvester, the generated voltage is proportional to the thickness of the piezoelectric layer (t_{xx}), the effective piezoelectric constant, $g_{31,f}$ (Vm/N), and the applied stress, σ_{xx}

$$V_{31} = \sigma_{xx} g_{31,f} t_{xx} \quad [16]$$

For typical values of $g_{31,f}$ and accelerations, the generated voltage becomes too small for the rectifying circuits as the thickness of the piezoelectric layer drops below 1 μm (mostly less than 0.5 μm) in MEMS–scale harvesters. Therefore, d_{31} mode of a piezoelectric device is often not favorable for energy harvesting applications even though the generated power could be higher. For high permittivity ferroelectric piezoelectrics, the d_{33} mode can generate higher open circuit voltages by increasing the spacing between the IDT electrodes where polarization wraps from one electrode to the next in alternating directions as shown in Figure 8. Jeon et al. showed that

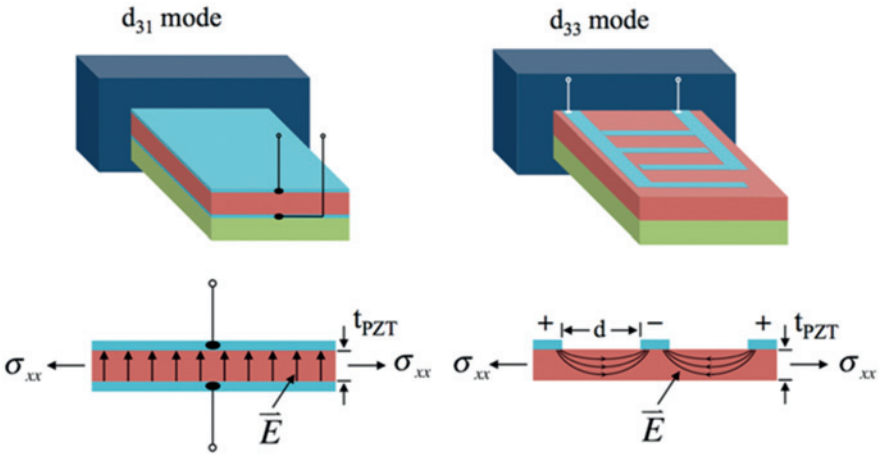

Figure 8: Two modes of piezoelectric conversion of input mechanical strain depending on the relative direction of the stress σ_{xx} (or strain) and the electric field, E. (Credit: Prof. Sang-Gook Kim).

operating piezoelectric elements in d_{33} mode is more advantageous than in d_{31} mode for MEMS-scale PZT harvesters (Jeon et al. 2005).

The power trapped in each cycle from eq. [9] is dissipated to structural and aerodynamic damping as well as to electrical energy via piezoelectric effect. To maximize the harvested power, the electrical damping needs to be increased while the structural and aerodynamic damping needs to be minimized. The electrical power generated via d_{33} mode piezoelectric effect of a unimorph cantilever can be expressed as:

$$P_{piezo} = V_{piezox} \cdot E_{piezo} \cdot s^2 \cdot \omega_{exc} \cdot k_{33}^3 \quad [17]$$

$$k_{33}^2 = \frac{Stored\ energy}{Input\ mechanical\ energy} = \frac{d_{33}^2 E_{piezo}}{\varepsilon_{piezo}} = \frac{e_{33}^2}{\varepsilon_{piezo} E_{piezo}} \quad [18]$$

where V_{piezo}, E_{piezo}, s, ω_{exc}, k_{33}, ε_{piezo}, and e_{33} are the volume of the piezo material, Young's modulus, strain, excitation frequency, electromechanical coupling coefficient, dielectric permittivity and piezoelectric coefficient. As long as the beam's stored energy minus the mechanical loss (dissipated via structural and aerodynamic damping), which can be defined as "extractable energy," is bigger than the "conversion energy" from eq. [17], the maximum harvested energy is determined by the piezoelectric layer's volume and coupling coefficient. Similar statement can be made for the d_{31} mode piezoelectric harvesters.

The coupling coefficient described in eq. [18] may only be applied to conditions where the passive elastic layer's stiffness can be neglected. For most MEMS energy harvesters with unimorph structure where the piezoelectric layer is much thinner compared to the passive elastic layer, eq. [18] may not be accurate. For an MEMS energy harvester, which consists of a thin layer of piezoelectric material and a much thicker passive elastic layer, the coupling factor can be written as (Xu and Kim 2012):

$$k^2 = \text{stored electrical energy/total input mechanical energy} = \text{stored electrical energy/(mechanical energy input to elastic layer + mechanical energy input to piezoelectric layer)} \quad [19]$$

It can be readily seen that only a portion of the input mechanical energy is injected into the piezoelectric layer to be converted into electrical energy, while much of the energy stays in the elastic layer as strain energy and will not be converted. Therefore, the coupling coefficient will be lower than the real intrinsic conversion rate of the piezoelectric material itself.

Figure of merit (FOM) for the piezoelectric materials can be derived by considering the power response of the piezoelectric transducer. Recently, Oliver and Priya have conducted detailed modeling of the piezoelectric cantilever (Bedekar, Oliver, and Priya 2010) and proposed a dimensionless figure of merit (DFOM) for piezoelectric transducer material in energy harvesting application as (Priya 2010):

$$\text{DFOM} = \left(\frac{k_{31}^2 Q_m}{s_{11}^E}\right)_{on-resonance} \left(\frac{d_{31} g_{31}}{tan\delta}\right)_{off-resonance} \quad [20]$$

where k_{31} is the transversal electromechanical coupling factor, Q_m is the mechanical quality factor, s_{11}^E is the elastic compliance at the constant field condition, d_{31} is the transversal piezoelectric strain constant, g_{31} is the transversal piezoelectric voltage constant, and tanδ

is the loss factor. The DFOM is a product of two FOM's representing off-resonance and on-resonance conditions.

By comparing DFOMs for the commercial piezoelectric compositions, one could identify the better piezoelectric composition for energy harvesting applications. Defosseux et al. have compared the off-resonance FOM for the PZT and AlN and noticed higher magnitude response for AlN (7.8×10^{-11} m^2/C as compared to 4×10^{-11} m^2/C) (Defosseux et al. 2012). For PZT, the values were taken to be $\varepsilon_{33}/\varepsilon_o = 935$, $d_{31} = -110 \times 10^{-12}$ m/V and $\tan\delta = 3.6\,\%$ (measured on PZT 53/47 [100]-textured 2 μm thin film (Ledermann et al. 2003)). For AlN, the values were taken to be $\varepsilon_{33}/\varepsilon_o = 10$, $d_{31} = -2.6 \times 10^{-12}$ m/V and $\tan\delta = 0.1\,\%$ (dielectric properties measured at 10 kHz for film with thickness of 2 μm by Martin et al. (2004) and piezoelectric property was reported by Tsubouchi and Mikoshiba for 1 μm thick film (Tsubouchi and Mikoshiba 1985). Considering the fact that AlN processing can be made compatible with CMOS, these results indicate the promise of AlN films towards developing MEMS harvesters.

2.6 Impedance Matching

Likewise the natural frequency matching with an external vibration source, the impedance of the piezoelectric generator should be matched to that of an external circuit in order to maximize the power extraction. Usually, an electrical impedance matching circuit is placed between the piezoelectric generator and external loads such as a rechargeable battery and supercapacitor. Thus, the matching network should be lossless and requires that the input impedance should be matched to the output impedance. Equation [21] shows the electrical input impedance of the energy source generated by the piezoelectric harvester.

$$Z = \frac{1}{2\pi\omega \cdot C_0} \qquad [21]$$

where ω is vibration frequency of energy harvester, C_0 is capacitance of piezoelectric materials. The impedance matching circuit consists of load resistors in accordance with the impedance of the piezoelectric generator calculated by eq. [21].

2.7 Challenges of Piezoelectric MEMS Energy Harvesters

Many piezoelectric MEMS energy harvesters have been developed and some of them are shown in Table 1. Their form factors are all different, and can only be compared with the power density which can be defined as the ratio of generated power over the active material volume (volume power density, μW/mm^3) or over the active material area (area power density, μW/mm^2). But, harvesters with high resonant frequency or that requires high acceleration ambient vibration need to be penalized considering the low frequency – low g characteristics of ambient vibrations. In order to generate a comparative figure, normalization was done with respect to both area and volume of harvesters, natural frequency and input acceleration.

Based upon eq. [16], the maximum extractable output power is proportional to (1/frequency) and (acceleration^2) (Chandrakasan et al. 1998). From eq. [17], the converted electrical power is proportional to the excitation frequency. Thus, some researchers have taken into account both frequency and acceleration variation, by normalizing the power with frequency or acceleration (Chandrakasan et al. 1998). We propose a simple metric for the normalization as Power / (frequency × acceleration^2 × area or volume) and refer to it as "areal or volumetric normalized power density" in this paper. Accordingly, a device generating higher power at lower frequency, acceleration and with area/volume will have higher normalized power density. For comparison, we utilized most common units used in literature to describe the physical quantities – Hz for frequency, mm^2 for area, and g^2 for acceleration. Table 1 is based on best estimates and data available in literature. Only the active piezoelectric area or volume is used to compute normalized areal power density (NAPD) and normalized volumetric power density (NVPD) depending upon the data availability in literature for MEMS devices developed using thin film deposition and lithography techniques.

For NAPD, harvester area (cantilever, non-linear beam, diaphragm, S-shape beam, corrugated beam, zigzag beam etc.) is calculated based on the data in the literature. We understand that energy harvested and transformed to electrical power is proportional to volume of piezoelectric material and hence volume may also be taken into account instead of area. For example, Hajati's non-linear beam energy harvester (Hajati and Kim 2011) showed 1–3 orders higher NVPD than that of any reported devices, but has a relatively low NAPD since it has very thin PZT (0.25 μm) over large area (120 mm). For battery-less operation of various wireless sensor nodes in real world applications, it will be ideal to harvest about 100 μW continuous power at the size of a quarter dollar coin (diameter = 24.26 mm, total thickness = 1.75 mm) at 100 Hz or lower ambient vibrations with less than 1 g

acceleration. This requirement can be converted to a NVPD (assuming one 0.5 μm thick piezoelectric layer in the device) = 4.3 μW/(mm^3·Hz·g^2). Most reported devices show orders of magnitude smaller normalized power density than this (See Table 1), even if we can increase the desired output power as increasing thickness of piezoelectric layer. One of the direct solutions to address this challenge is to improve the electro-mechanical coupling coefficient of the piezoelectric thin films. Another approach is to seek new resonating beam structure designs from which more energy can be extracted at lower frequency and acceleration.

Another metric commonly used in literature is normalized figure of merit, which takes into account bandwidth. Bandwidth is also an important characteristic and should be accounted for determining the performance of piezoelectric harvesters under unpredictable or uncontrollable spectra of ambient vibrations. Most piezoelectric energy harvesters have been designed based on a linear resonator, e. g. a cantilever with a proof mass. The extractable power of an energy harvester based on a linear resonator is proportional to the gain (quality factor, $Q = f_r/\Delta f$ where f_r is resonance frequency, Δf is full width at half maximum) of the resonator, which is inversely proportional to the bandwidth. If the center frequency of a beam is off about 2% from the input frequency, the amplitude of the beam bending drops to about 50% of the resonance peak. If it is off 5%, then there is no resonance to amplify the strain on the piezoelectric material. Accordingly, there is a trade-off between the output power and the bandwidth. Since we cannot control the frequency of ambient vibrations, an energy harvester with a narrow bandwidth (of most linear resonators) is impractical in most real applications. Several approaches have been adopted to circumvent this gain-bandwidth dilemma. For example, the natural frequency of resonating beams can be tuned by changing the axial tension of a beam through non-contact mechanisms such as magnetic attractive and repulsive forces. Beam dimensions and proof mass have also been tuned mechanically to widen the bandwidth. (Al-Ashtari et al. 2012; Mansour, Arafa, and Megahed 2010). However, frequency tuning inevitably consumes power, the tuning efficiency is low and the tuning range is limited. Multiple beams of different lengths have also been utilized to address this challenge, which may not be practical in terms of size and cost. Simpler and less costly methods have been sought that can provide both the wide bandwidth and high power density as required for practical MEMS-scale devices.

3 Recent Advances in Piezoelectric MEMS Energy Harvesting

In order to address the challenges described above, advances have been made both in improving the performance of piezoelectric materials and design of resonating beam structures to achieve higher power density and wider bandwidth.

3.1 Grain Textured and Epitaxial Piezoelectric Films

Bulk PZT ceramics have plethora of dielectric and piezoelectric properties which can be controlled using doping (Funakubo et al. 2012). Lead based relaxor-lead titanate compounds so called relaxor ferroelectrics include Pb$(Zn_{1/3}Nb_{2/3})O_3$-$PbTiO_3$(PZN–PT), Pb$(Mg_{1/3}Nb_{2/3})O_3$-$PbTiO_3$ (PMN–PT) and Pb$(Y_{1/2}Nb_{1/2})O_3$-$PbTiO_3$(PYN–PT), exhibit large electromechanical coupling coefficients which makes these materials more attractive option for micro-actuator and micro-sensor applications. For device miniaturization it is important to grow films using these materials. PZT thin films are deposited with variety of methods such as sputtering, chemical solution deposition (i. e. sol-gel), MOCVD and laser ablation processes. Since piezoelectric properties of these materials are strongly dependent on film quality and growth orientation, thus, the control of growth orientation is highly desired with (001) texturing (Trolier-McKinstry and Muralt 2004). Additionally, the composition of the piezoelectric material plays a crucial role in deciding the piezoelectric properties of films. For example, in case of PZT thin films, composition near the morphotropic phase boundary (MPB) is commonly preferred due to its high piezoelectric response (Jaffe 1971). From application point of view, it is very important to integrate these oxides on Si substrates which could pave the way for efficient fabrication of devices. However, the growth of oxide films on Si substrate is still a complicated process due to technical difficulties such as inter-diffusion, large lattice mismatch, and thermal expansion mismatch (Chopra et al. 2013). Tremendous efforts have been made to integrate the oxide films on Si substrate with control of crystal orientation.

The most simple and direct solution towards enhancing the output power at the fixed size of a device is to increase the piezoelectric and electromechanical coupling coefficient. Grain texturing has been shown to be

an effective method for improving the magnitude of physical constants in piezoelectrics by achieving a domain-engineered state. In the vicinity of morphotropic phase boundary, a rhombohedral composition oriented along <100> direction is known to exhibit optimum magnitude of electromechanical coefficients (Du et al. 1998). Park and Shrout attributed this high electromechanical performance to domain engineered state achieved through polarization rotation from <111> to <100> (Park and Shrout 1997). Thus, texturing is desired in PZT but poses several challenges in synthesis.

An important characteristic in driving the texture of complex oxides on Si substrates is proper texturing of the electrode layers. Most commonly, Pt electrodes are employed for many applications and achieving highly (111) textured Pt films on Si requires proper control of the adhesion layer, typically TiO_2. Recent efforts have identified the importance of surface roughness of the underlying passive elastic layers (commonly SiO_2), residual oxygen content during the Ti sputtering process, sputter temperature, Ti thickness, and high temperature oxidation of the Ti into textured TiO_2 as critical parameters enabling a nearly pure (111) textured Pt layer with a FWHM ranging from 1.5 to 2.5 degrees (Potrepka et al. 2011). Combining a highly textured Pt electrode with proper seed layer can be used to achieve (001) texture (Sanchez et al. 2013).

In addressing the optimization of synthesis conditions, Temperature-Time-Transformation (TTT) diagrams have been proposed to document texture evolution during thermal treatment of PZT thin films on platinized silicon substrates (Varghese et al. 2011). By varying the annealing/pyrolysis temperature and time, extensive exploration of the sol-gel thermal budget operating space yielded the TTT diagram as shown in Figure 9(a)–(c). It can be seen that films with pyrolysis at 300 °C for 3 min were textured in (100) direction until >750 °C annealing temperature, after which they start showing random orientation. On the other hand, the films pyrolyzed at lower temperature and for shorter times are textured in (100) direction for a narrow threshold annealing temperature range. Ternary diagram [Figure 9(d)] illustrates the frequency of each textured orientation obtained for each pyrolysis binned as per the ranges in annealing temperature and time. Thus, one is able to quantify the operating regime for achieving specific texture orientation. These diagrams are also invoked to understand the texturing mechanism (Chen and Chen 1994) and can be further expanded to include other piezoelectric materials system (Zhou, Apo, and Priya 2013a).

Several studies in literature have been conducted on tuning the piezoelectric properties through interfacial stress. Recent results by Han et al. have shown ~90 % enhancement of ferroelectric and piezoelectric properties in MPB composition PZT thick films by tailoring the magnitude of residual stress by choosing substrates with different coefficient of thermal expansion. The results from this study are summarized in Table 4 (Brennecka et al. 2004; Han et al. 2011a; Tuttle et al. 1992; Yokoyama et al. 2002). The direct piezoelectric constant ($d_{33,\ eff}$, pC/N) was measured by d_{33} meter and the effective piezoelectric constant ($d_{33,\ eff}$, pm/V) was obtained by measuring variation in displacement with applied electric field using laser interferometer. The difference between these two coefficients is attributed to the substrate clamping effect. The electrical properties showed that the films on Yttria stabilized Zirconia (YSZ) substrates with highest in-plane compressive stress had the best piezoelectric properties while that on Si wafer with tensile in-plane compressive stress showed lower properties. The enhanced piezoelectric properties were attributed to the reason that c-domain parallel to the thickness were easy to form under in-plane compressive stress. This technique is quite appealing as it can be easily implemented in the fabrication of MEMS components.

Epitaxial PZT thin films with c-axis orientation are excellent materials for MEMS energy harvesters (Kanno et al. 1997; Morimoto et al. 2010). However, epitaxial substrates, such as MgO and $SrTiO_3$, are usually not suitable for unimorph cantilevers because of their brittleness and difficulty of microfabrication. One of the solutions is transferring the epitaxial PZT films on flexible cantilevers. Qi et al. transferred epitaxial PZT thin films deposited on MgO substrates to PDMS substrates and have evaluated performance of stretchable piezoelectric energy harvester (Qi et al. 2011). Morimoto et al. have developed high efficiency piezoelectric energy harvesters using c-axis oriented PZT thin films by radio-frequency (rf)-sputtering, which were transferred onto stainless steel (Morimoto et al. 2010). The fabrication process from this study is shown in Figure 10. The c-axis oriented PZT thin films were grown on (100) MgO single crystals with an epitaxial (001) Pt bottom electrodes. Reciprocal lattice space maps before and after transfer process clearly showed spotty diffractions of the (204) PZT, indicating that the transfer process did not degrade the crystal structure of the epitaxial PZT film. After the PZT film was bonded to 50-μm-thick stainless steel sheets with epoxy resin, the MgO substrate was etched out in

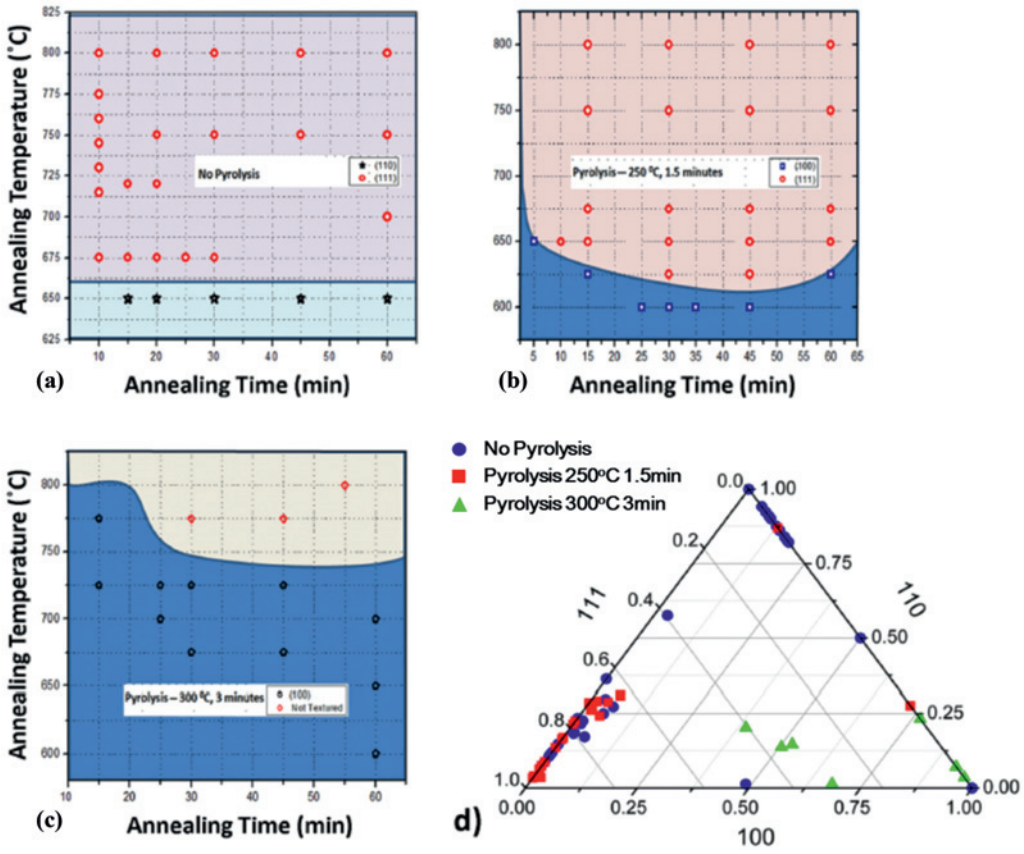

Figure 9: Temperature-time-transformation diagrams of PZT-sol-gel thin films pyrolyzed at (a) no pyrolysis; (b) 250 °C, 1.5 min; (c) 300 °C, 3 min; and (d) the ternary plot of all the data. (Varghese et al. 2011).

Table 4: Relationship between in-plane stress and electric/piezoelectric properties in PZT thick films deposited on various substrates (Han et al. 2011a).

Substrate	In-plane Stress [MPa]	d_{33}^{eff} [pC/N]	d_{33}^{eff} [pm/V]	ε_r [1 khz]	*tan δ* [1 khz]	$\Delta P_r/2$ [μC/cm^2]	$\Delta E_c/2$ [kv/cm]
Silicon	119.5 ± 4.1(tensile)	50	26.4	1026	0.025	17.0	52.6
Sapphire	−131.5 ± 1.1(compressive)	80	59.8	1260	0.023	23.4	37.4
YSZ	−270.6 ± 4.9(compressive)	95	66.1	1265	0.039	25.5	30.0

phosphoric acid. The photograph of the stainless steel cantilever beam covered with the epitaxial PZT is shown in Figure 10. The relative dielectric constant ε_r of the transferred films on stainless steel was as low as 166, while the piezoelectric coefficients $e_{31,f}$ of the transferred PZT films was around −6 C/m^2. The thickness and length of stainless steel cantilever was 50 µm and 18.5 mm respectively. Because of the thin dimension of the metal cantilever, the first resonance was found to occur at 126 Hz. Averaged output voltage and calculated value are plotted in Figure 11 (acceleration: 5 m/s^2). The maximum output electric power of 5.3 µW was obtained across a load resistance of 50 kΩ. In this measurement, GEMC, k_G^2 was calculated to be 1.3×10^{-2} which is much larger than polycrystalline PZT thin films on Si substrates. This result is attributed to large electromechanical coupling coefficient k_{31} of epitaxial PZT thin films. The output power increases monotonically with the acceleration, reaching 244 µW at 50 m/s^2. The flexible metal cantilever enables considerable reduction of the resonant frequency and offers enhanced toughness compared with brittle Si-based cantilevers.

Recently, direct deposition of PZT thin films on Nickel foil for MEMS energy harvesters have been

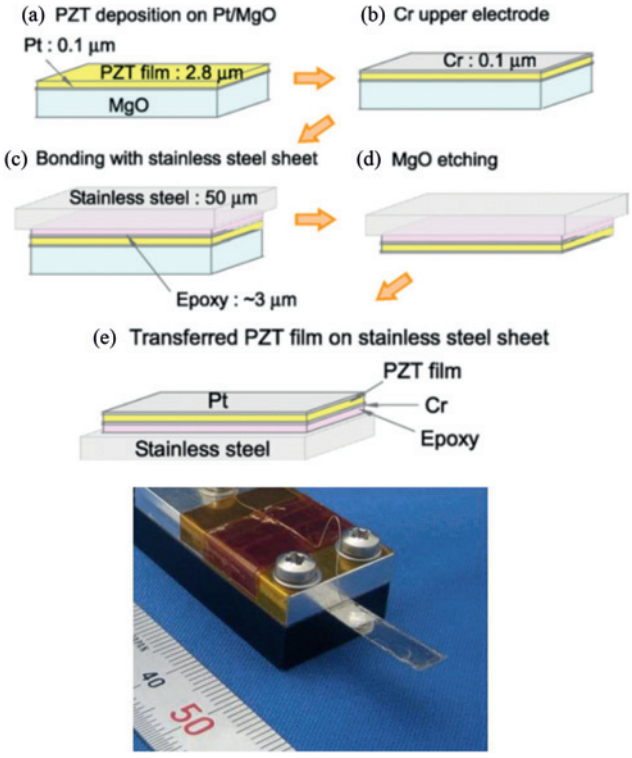

Figure 10: Fabrication process flow and photograph of transferred epitaxial PZT thin films on stainless steel cantilever (Morimoto et al. 2010).

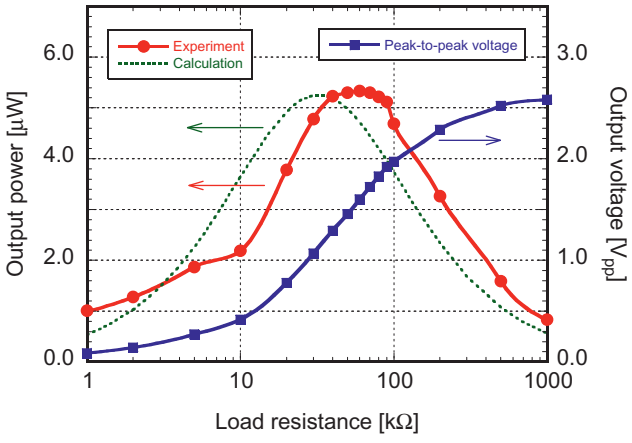

Figure 11: Output voltage and generated power of transferred epitaxial PZT thin films as a function of load resistance (Morimoto et al. 2010).

successfully demonstrated by Yeo and Trolier-McKinstry (2014). (001) oriented PZT thin films were grown by sol-gel process on Ni substrate. HfO_2 and (001) oriented $LaNiO_3$ films were used as a passivation layer to suppress the substrate oxidation and buffer layer to subsequently grow (001) oriented film, respectively. Surface and cross-sectional microstructure images of PZT films on Ni are shown in Figure 12(a) and (b). The PZT film have columnar structure and there was no evidence of cracks or delamination among layers as shown in Figure 12(b). The permittivity and loss tangents of (001) oriented PZT films on Ni are near 780 and 0.04 at 1 kHz. The PZT film on Ni foil displayed a well-saturated hysteresis loop with a large remanent polarization of ~36 μC/cm^2, while the (100) oriented PZT on Si substrate showed much lower remanent polarization as plotted in Figure 13. In addition, this PZT film on Ni had a large transverse piezoelectric constant $e_{31,f}$ of −10.6 C/m^2. This PZT film directly grown on metal substrate is favorable for a low resonance frequency and robust MEMS energy harvester.

Epitaxial growth of ferroelectric thin films on silicon suffers minimal leakage and optical scattering which results in a drastic improvement of electrical properties when compared to polycrystalline films. Thus epitaxial integration of ferroelectric films such as PZT, PST ($PbSc_{0.5}Ta_{0.5}O_3$) on Si substrate is highly desirable for the development of next generation devices. However, direct integration of PZT on Si using Pulsed laser deposition (PLD) still remains a challenging task due to interdiffusion, structural and chemical incompatibilities, and thermal and lattice mismatch issues. These issues can be addressed using buffer layers such as $SrTiO_3$ and yttria-stabilized zirconia (YSZ)/CeO_2 (Chopra et al. 2013; Du et al. 1998). These buffer layers act as diffusion barrier as well as help in bridging the lattice mismatch between film and substrate. PLD is one of the preferred methods for fast deposition of high quality films. Zirconium (Zr) is one of the few metals which has a higher affinity towards O_2 than Si. This makes YSZ inert to Si and prevents oxidation of Si during deposition in O_2 atmosphere. CeO_2 is another buffer layer which is employed in combination with YSZ to reduce the lattice mismatch further. Successful integration of functional oxides on Si substrate has been reported in literature (Chopra et al. 2013, Chopra, Alexe, and Hesse 2015a; Gardeniers, Smith, and Cobianu 1995). (001)-oriented growth of oxides is achieved by fabricating Si (100)/YSZ/CeO_2/$LaNiO_3$ structures (Chopra et al. 2013). The orientation of the films can be switched from (001) to (110) just by replacing the heterostructure with Si (100)/YSZ/$SrRuO_3$. $LaNiO_3$ and $SrRuO_3$ both act as a bottom electrode in their respective heterostructures, which are necessary for the electrical measurements. The XRD measurements performed on such heterostructures reveal a (001) and (110)-oriented growth as shown in Figure 14.

The in-plane XRD scans confirm that both the discussed structures are epitaxial, however LNO and subsequent layers in the (001)-oriented heterostructure were

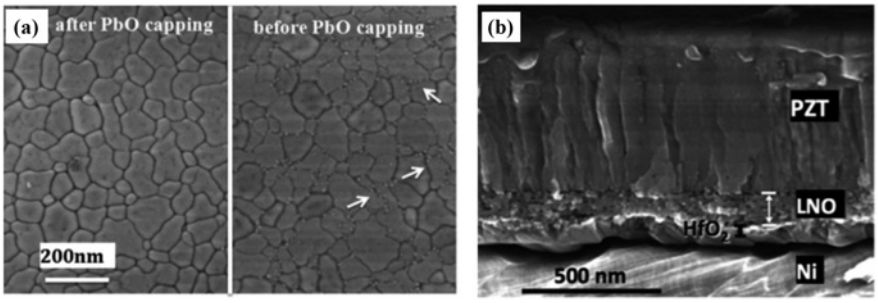

Figure 12: (a) Surface and (b) cross-sectional SEM images of PZT films deposited on LNO (100 nm)/HfO_2 (30 nm)/Ni foil after PbO-precursor cover coat (Yeo and Trolier-McKinstry 2014).

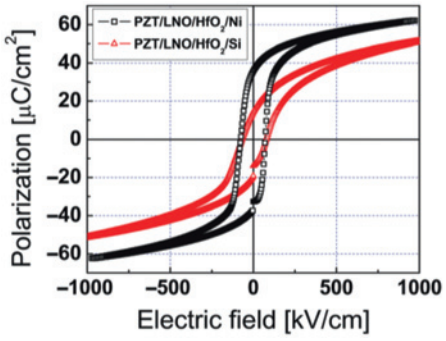

Figure 13 : P-E hysteresis curves of (001) oriented PZT (52/48) films on Ni and silicon substrates respectively (Yeo and Trolier-McKinstry 2014).

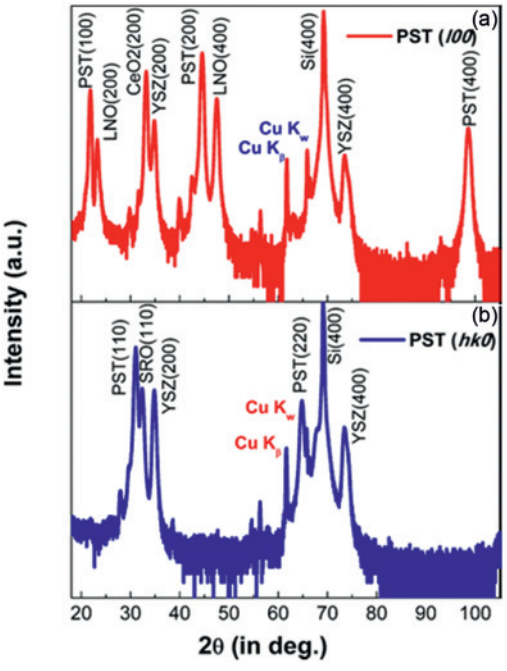

Figure 14: Out of plane XRD patterns obtained from the PST films deposited on (a) LNO/CeO_2/YSZ/Si, (b) SRO/YSZ/Si (Chopra, Alexe, and Hesse 2015a).

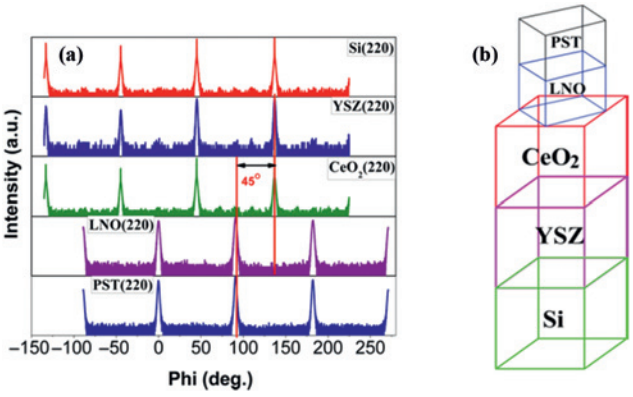

Figure 15: (a) In-plane φ-scan for PST on LNO/CeO_2/YSZ/Si showing LNO and PST has 45 ° in-plane rotation with respect to CeO_2/YSZ/Si. (b) A schematic showing the 45 ° rotation (Chopra et al. 2013, Chopra, Alexe, and Hesse 2015a).

found to be rotated in plane by 45 degrees with respect to the underlying YSZ and CeO_2 layers as shown in Figure 15(a). This kind of in-plane rotation is facilitated due to good arrangement in the lattice parameters of both CeO_2 ($a = 0.541$ nm) and LNO ($a_{pc} = 0.386$ nm) which resulted in an in-plane rotation for the top ferroelectric layer too.

Recently successful integration of PZT films on glass substrates using 2D nanosheets has been demonstrated (Chopra et al. 2015b; Jumpertz et al. 2014). The biggest advantage of using nanosheets is reduction in growth temperature. Crystalline growth of YSZ, CeO_2 and $SrTiO_3$ buffer layers is achieved at very high temperature of 750 °C which is not suitable for substrates like glass. Thus, low temperature growth of buffer layers was achieved by replacing the oxide buffer layers with nanosheets which grow at room temperature. The nanosheets were transferred to the substrates using langmuir-blodgett deposition process. The orientation control of PZT films was achieved using $Ca_2Nb_3O_{10}$ (CNO) and $Ti_{0.87}O_2$ (TO) nanosheets. A (001)-oriented growth of LNO films was achieved using CNO nanosheets due to the

exact lattice match between CNO nanosheets (lattice parameter = a = 3.86 Å) and LNO (lattice parameter = a = 3.86 Å) which further promoted a (001)-oriented growth of subsequent PZT thin films. On the other hand, TO-nanosheets which are known to have a lepidocrocite-type structure with a lattice parameter of $a = 3.76$ Å and $b = 2.97$ Å promotes (110)-oriented growth of both LNO and subsequent layer of PZT as shown in Figure 16(a). However, all the films deposited were polycrystalline due to random in-plane distribution of nanosheets. Growth of nanosheets with single orientation in in-plane direction is the next challenge in the field which is being addressed to achieve a complete epitaxial growth of subsequent layers. Fatigue and piezoelectric measurements demonstrated on nanosheet buffered PZT films showed stable and good piezoelectric properties which are essential for the stable operation of the next generation devices. A comparison of the piezoelectric response of PZT films on nanosheets and Pt is shown below in Figure 16(b).

It is well-known that relaxor ferroelectric single crystals, such as PMN-PT and PZN-PT, show about 10 times larger piezoelectric coefficient than that of conventional PZT ceramics (Kuwata, Uchino, and Nomura 1982; Park and Shrout 1997). Recently, Baek et al. successfully grew epitaxial PMN-PT thin films on $SrTiO_3$–buffered miscut Si substrate by off-axis sputtering. The piezoelectric coefficient $e_{31,f}$ in their work was reported to be -27 C/m^2, which is the highest value reported (Baek et al. 2011). Using these films, they fabricated a unimorph micro-cantilever and confirmed the excellent inverse piezoelectric performance. Because of the large electromechanical coupling coefficient k_{31} (or figure of merit: $e^2_{31,f}/\varepsilon_r$) of PMN-PT epitaxial thin films, this system is quite promising towards improving the performance of current MEMS energy harvesters.

3.2 Lead-Free Piezoelectric Films

For powering medical implants and human use of energy harvesters, lead-free piezoelectric material is desirable. Potassium sodium niobate ($K_xNa_{1-x}NbO_3$) abbreviated as KNN, is considered as a most promising lead-free piezoelectric material owing to its higher Curie temperature and higher ferroelectric orthorhombic – ferroelectric tetragonal transition temperature (Ahn et al. 2008a). The piezoelectric properties of KNN based compositions are directly correlated to the fraction of orthorhombic (O) and tetragonal (T) phase as shown in Figure 17(a). One of the strategies for achieving higher piezoelectric response has been to modulate the composition such that O/T transition lies close to room temperature (Ahn et al. 2008b). Another strategy adopted for designing lead-free compositions is based upon the trend between atomic weight ratio of A to B sites ($R_w = W_a/W_b$) and longitudinal piezoelectric constant d_{33} as shown in Figure 17(b) (Ahn et al. 2009). It can be observed that $1/R_w$ for KNN ceramics (for Na/K ratio of 0.5) is similar to R_w for PZT ceramics at MPB composition and both of these materials exhibit high piezoelectric response. Piezoelectric compositions show large response when R_W for A-site heavy perovskites and $1/R_W$ for B-site heavy perovskites is higher than 2.0.

The fabrication process of these lead-free piezoelectric materials in thin-film form is still under development, and it is expected that these materials will be utilized in the design of MEMS energy harvesters in the near future (Zhou et al. (2013b)). Recently, Shibata et al. reported that KNN thin films deposited by RF magnetron sputtering showed large transverse piezoelectric properties comparable to those of PZT thin films (Shibata et al. 2011). Kanno et al. have compared the energy harvesting performance of KNN thin films with PZT thin films by using simple

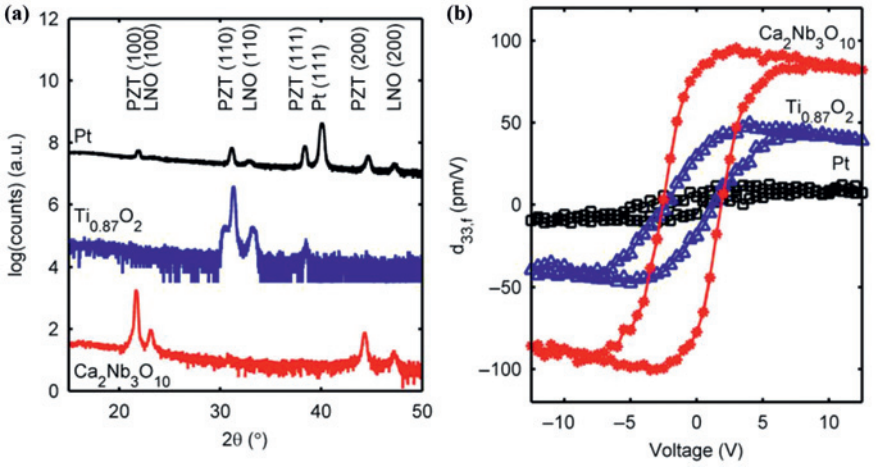

Figure 16: (a) Out of plane (θ–2θ) scans and (b) Longitudinal piezoelectric response of the PZT films deposited on Pt, $Ti_{0.87}O_2$ and $Ca_2Nb_3O_{10}$ buffer layers coated on glass substrate (Bayraktar et al. 2014).

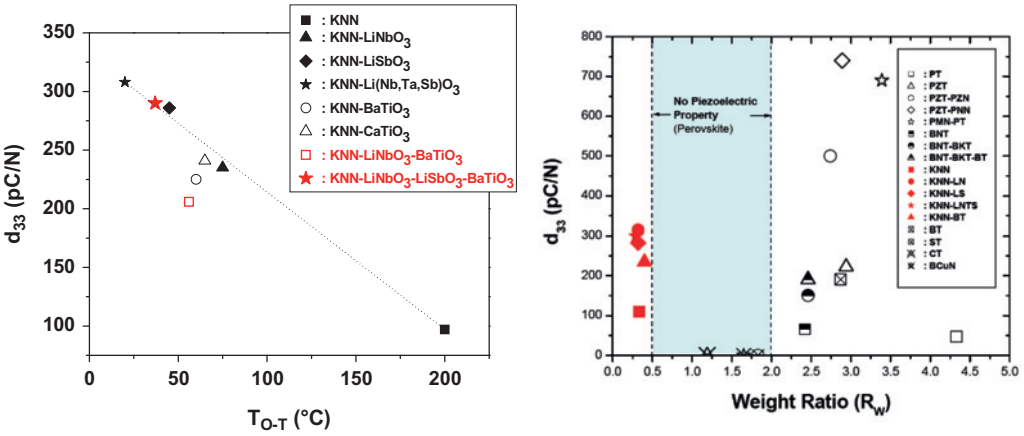

Figure 17: (a) Variation of longitudinal piezoelectric coefficient with O–T transition temperature in KNN system, and (b) Variation of longitudinal piezoelectric coefficient as a function of weight ratio in bulk perovskites (Ahn et al. 2008b).

unimorph Si-cantilevers (Kanno et al. 2012). The piezoelectric coefficient of both KNN and PZT films showed almost the same value of $e_{31,f} = -10\ \mathrm{C/m^2}$ (Kanno et al. 2012). The relative dielectric constants of the KNN and PZT films were 744 and 872, respectively. Figure 11 shows the average output power $P = V^2/(2R)$ as a function of load for energy harvesters made of KNN and PZT unimorph cantilevers. Measurements were performed at the resonance frequency of each cantilever (KNN: 1.0 kHz, PZT: 0.89 kHz; acceleration 10 $\mathrm{m/s^2}$). Peak output power for the KNN and PZT films was 1.1 µW at 1.7 kΩ and 1.0 µW at 1.2 kΩ, respectively. Because KNN and PZT thin films have almost same dielectric and piezoelectric properties, the KNN film performs comparably to the PZT film with respect to power generation. GEMC k_G^2 of KNN and PZT energy harvesters was around 0.6 ~ 1.7×10^{-3} as determined by fitting the calculated value of eq. [12] to experimental results.

3.3 Aluminum Nitride (AlN) – A MEMS Compatible Piezoelectric Film

AlN is a piezoelectric material with wurtzite structure. The properties of AlN based films are highly process dependent. Aluminum nitride has a band gap of 6.2 eV with lattice parameter of $a = 13.112$ Å and $c = 4.982$ Å. It is a potential candidate for UV light emission and SAW devices due to large acoustic wave (SAW) velocity (Duffy et al. 1973). AlN films have been deposited using chemical vapor deposition (CVD) (Chubachi, Sato, and Kojima 1984), plasma assisted CVD (Zhang et al. 1993), metalorganic CVD (Saxler et al. 1994), reactive DC-magnetron sputtering (Meng, Heremans, and Cheng 1991), plasma assisted molecular beam epitaxy (MBE) (Stevens et al. 1994), laser-induced chemical vapor deposition (Li and Tansley 1990), and pulsed laser deposition (Norton, Kotula, and Carter 1991). Most of these techniques required a high processing temperature (1,000 °C) to obtain the best crystal quality and texture in the deposited thin films. However, high quality growth at low temperature is desired to ensure the compatibility with IC technology. In this regards, different process techniques have been developed (Aita 1982; Shiosaki et al. 1980; Takeda, Mori, and Takahashi 1981). In addition to (0001)–orientation, it is also observed that tuning of the ion energy and flux of the bombarding ions (Ar^+, N^{2+}) is equally important (Dubois, and Muralt 2001). AlN films have a much higher phase velocity and chemical stability in comparison to the ZnO films. However, AlN has lower piezoelectric coupling and it is difficult to control the growth of AlN films.

Recently, significant progress has been made towards incorporating the AlN films in energy harvesting applications. Schaijk et al. have demonstrated the performance of micomachined AlN cantilevers and shown that device with dimension of 3 × 1.3 mm was able to provide 10 µW at the resonance frequency of 1,155 Hz under 8 g acceleration (Van Schaijk et al. 2008). Under practical acceleration values of 1 g or lower, the power generated was smaller than 1 µW. Heidrich et al. have investigated the energy generation from [001] textured AlN cantilevers and corrugated membranes for bio-implants. The growth was conducted on Si (001) substrates, which resulted in tensile (< + 300 MPa) and compressive strains (>–100 MPa) depending upon the deposition parameters. In the non-resonant condition of 70 Hz, for a 3 × 4 corrugated membrane array (radius of individual membrane = 400 µm) the

peak power of 10 μW was measured across 10 kΩ with a bias of 1 V and acceleration of 0.01 g (Heidrich et al. 2011). Yen et al. conducted detailed experimentation and modeling of the corrugated AIN cantilever structures. At a resonance frequency of 853 Hz, a cantilever with a width of 2,400 μm, length of 500 μm, and a 2 μm thick piezoelectric layer was able to provide 0.17 μW under an acceleration of 1 g using a tip mass of dimension 2,400 × 500 × 680 μm (Ting-Ta et al. 2011). Andosca et al. also demonstrated a AlN thin film based MEMS energy harvester with high power density. The energy harvester with a width of 6.0 μm, length of 7.8 μm, a 2 μm thick AlN film and a proof mass of 28.9 mg was able to generate 119 μW power under 1 g acceleration at a resonance frequency of 56.6 Hz (Andosca et al. 2012).

A simulation study in this area has been conducted by Stoppel et al., who computed the effect of thickness on power generation (Stoppel et al. 2011). It was pointed out that since the Young's modulus of AIN (345 GPa) is about 4× that of PZT, the thickness of AIN for maximum power output is about 3× smaller than that of PZT. For a cantilever with 2 μm thick AIN operating at resonance frequency of 105.6 Hz under acceleration of 1 m/s^2, output power of 0.8 μW was measured across 21 MΩ load. Based upon the experimental data available in literature, the normalized output power (power/frequency × acceleration) for AIN micro devices ranges between 2.034×10^{-5}–757×10^{-5} μW/(Hz × m/s^2). Ignoring the data from Stoppel et al., the spread is more reasonable 2.034×10^{-5}–11×10^{-5} μW/(Hz × m/s^2). These values are quite good and considering the compatibility of AlN with CMOS process and long history in optimizing the deposition process, we expect that this area will continue to grow.

3.4 Piezoelectric Thick Films by Powder/Granule Spray in Vacuum Process

The powder spray in vacuum process so called aerosol deposition (AD) is a unique ceramic film deposition technology that is able to fabricate highly dense thick films (submicron to several hundred μm) at room temperature. This process utilizes high kinetic energy of ejected aerosol consisting of a mixture of fine ceramic particles and carrier gas from a nozzle. The process was firstly introduced by Akedo and co-workers at AIST, Japan in late 1990s (Akedo and Lebedev 2000). The process has unique advantages compared to other thin/thick film deposition process such as high deposition rate (over several tens μm/min depending on the deposition area), low processing temperature, composition control, high adhesion strength between substrate and film as well as micropatterning of ceramic thick films during deposition (Zhou et al. 2011). Due to its low temperature processing, low sinterability ceramic thick films such as KNN based lead-free piezoelectrics and $PbTiO_3$ ceramics with full density can be deposited on various types of substrates (Han et al. 2011b; Ryu et al. 2007, 2014; Wang et al. 2008). Figure 18 shows ferroelectric/piezoelectric property modulation of AD-PZT film according to the variation of residual stress level (Han et al. 2011a). By generating high compressive residual stress in the PZT thick films, the piezoelectric properties can be enhanced by ~2 ×. All these advantages are highly attractive for MEMS based piezoelectric device applications as mentioned in previous section.

Lee and co-workers at National Taiwan University reported the MEMS devices based upon the AD process in 2008 (Lee et al. 2009; Wang et al. 2008). Figure 19 represents their device pictures. By using AD process, they succeeded to fabricate over 10 μm PZT thick film on the silicon wafer and realized MEMS energy harvesters and other piezoelectric devices. The output power from their MEMS energy harvester with AD PZT was in the vicinity of 2 μW at ~ 255 kHz under 2 g acceleration. This is reasonably good performance compared to the other MEMS based piezoelectric energy harvesters (Lee et al. 2009).

Park and co-workers at KIMS, Korea, have been conducting detailed study on optimization of deposition rate and uniformity in large area films by the granule spray in vacuum process. They have succeeded to overcome the limitation of AD by using intentionally granulated raw powder and feeding system, termed as 'granule spray in vacuum process (GSV)'. Figure 20 shows the typical microstructure of patterned highly dense PZT thick films for MEMS ultrasonic transducers by GSV. The deposition rate of the PZT thick film by GSV was 1.4 μm/min in the area of 1440 cm^3. That is over two orders of faster rate than that of the other thin film processes. The film was very uniform as shown in Figure 20(a). Directly patterned highly dense 11 μm thick PZT film was fabricated on 6 inch $Si/SiO_2/Ti/Pt$ wafer by GSV, and the films were not damaged during post processes including back-DRIE process.

3.5 Nonlinear Resonance Based Energy Harvesting Structures

Most of the reported vibration energy harvesters use a linear cantilever resonator structure to amplify small ambient vibration. While such structures are easy to

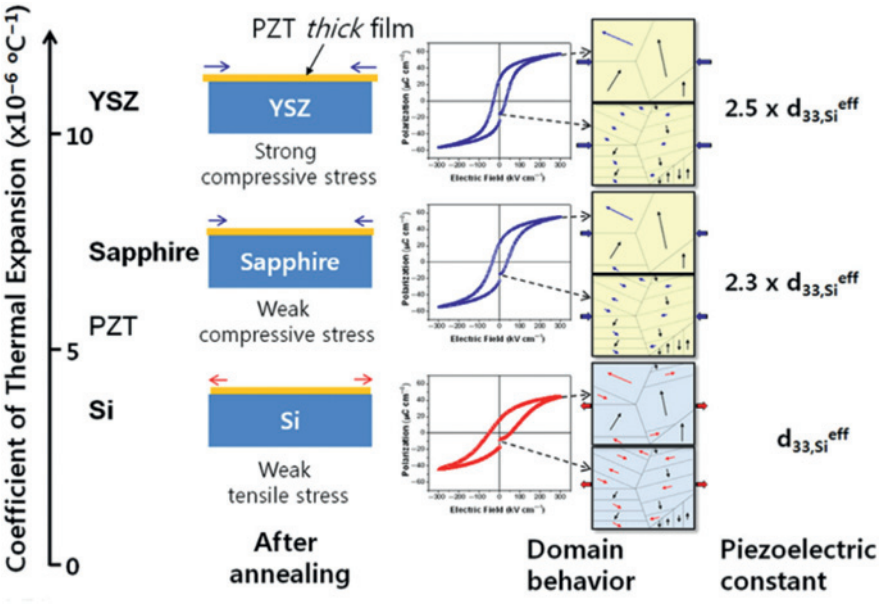

Figure 18: Conceptual diagram of high piezoelectric performance in PZT thick films grown on various substrates; the stresses were controlled by the thermal expansion mismatch between substrates and PZT films (Han et al. 2011a).

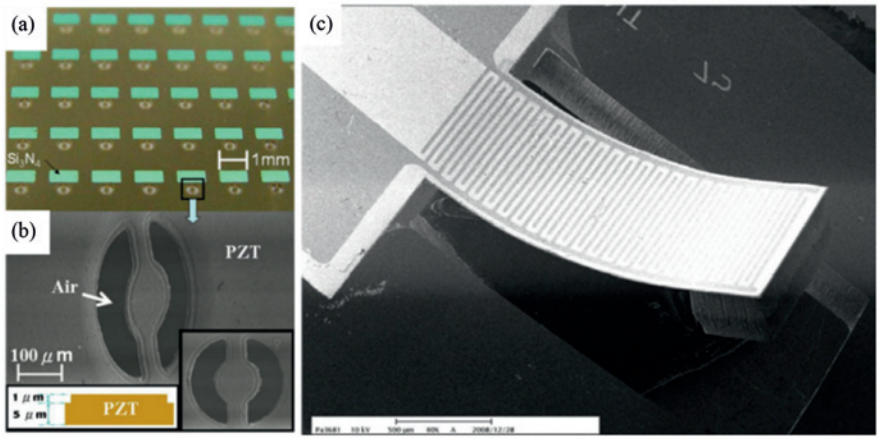

Figure 19: Silicon based MEMS devices with AD-PZT by Lee et al. (a), (b) Suspended double-layer PZT structure released by XeF_2 dry etching (Wang et al. 2008), (c) piezoelectric MEMS energy harvester with AD-PZT thick film (Lee et al. 2009).

model, design and build, they typically have a narrow bandwidth. In contrast, nonlinear resonators have different dynamic response and greatly increase the bandwidth by hardening or softening the resonance characteristic of the beam structure. In addition, it has been found that non-linear resonating beams can extract more electrical energy than that of linear resonating beams (Hajati and Kim 2011; Marinkovic and Koser 2009) when external vibration source has variable frequency.

Nonlinearity may come from magnetic force or constrained mechanical structures. The magnetic forces between the magnets and the iron create a nonlinear spring, whose nonlinearity is determined by the strength of the magnets and the size of the air gap between the magnets and the iron stator. Due to the mutual attractions, the ferromagnetic beam has three equilibrium positions (statically bi-stable configuration), and the vibration mode has the form of the bi-stable *Duffing* resonance. Electromagnetic energy harvesters have been reported showing hardening or softening resonance characteristics (Ando et al. 2010; Barton, Burrow, and Clare 2010; Erturk and Inman 2011; Mann and Sims 2009). However, magnet-based beams require assembly of hard magnets, which is expected to be costly as the size of the device shrinks.

Nonlinear resonance could be better achieved by a monolithically fabricated MEMS structures. Efforts have been made to achieve wide bandwidth piezoelectric

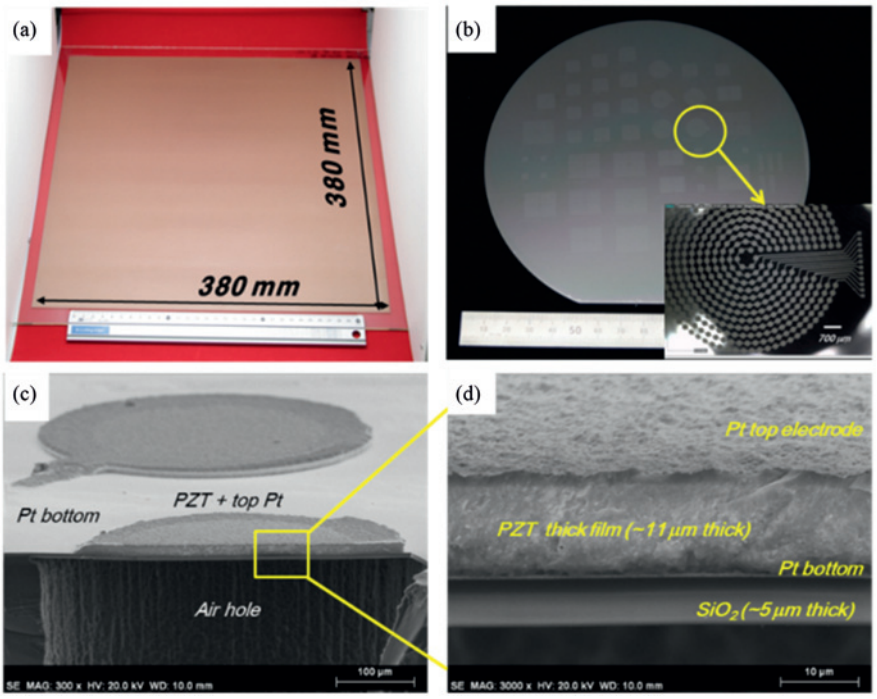

Figure 20: (a) Large area PZT deposition by GSV process. (b) 6 inch $Si/SiO_2/Ti/Pt$ wafer with directly patterned PZT thick film. (c) and (d) cross-sectional SEM micrographs of piezoelectric MEMS ultrasonic device by GSV.

energy harvester by exerting an axial compression and forming a buckled configuration, to make a bi-stable oscillator (Cottone et al. 2012; Marinkovic and Koser 2009). Recently, Hajati et al. demonstrated a monolithic MEMS-based non-linear resonant piezoelectric micro energy harvester, which achieved an ultra-wide bandwidth of >>20 % of the center frequency and generated power more than 22 μW (see Figure 21) (Hajati and Kim 2011). More than one order of magnitude improvements were demonstrated in comparison to the devices previously reported in both the power bandwidth and the normalized power density (NPDV) (see Table 1). The basic design is based on a doubly clamped beam resonator with dimensions, 6 mm × 6 mm × 5.5 μm ($L \times W \times H$), PZT thickness 0.25 μm. Four of these resonators are arranged perpendicular to each other and form one energy harvester, which is about the size of a US quarter coin (Figure 21(a)). At large deflection (exceeding 2–3 times the thickness of the beam), a net stretching in addition to bending results, which changes the dynamic response to a non-linear one (Figure 21(b)).

Unlike a linear resonance system, where the electrical damping cannot exceed the mechanical damping (Dutoit, Wardle, and Kim 2005), it has been shown that electrical damping in a nonlinear resonance system could surpass the mechanical damping, extracting much higher output power than that of the linear systems. The nonlinear impedance serves as a negative feedback and stabilizes the deflection when the electrical damping changes (Hajati, Xu, and Kim 2011). This is why the power bandwidth of nonlinear systems can be much wider than that of linear systems at equivalent beam dimensions.

Bi-stable nonlinear resonant beams were recently developed not only to widen the power bandwidth but also to lower the working frequency range and input vibration amplitude of energy harvesters (Xu and Kim 2015). Electromechanical lumped model predicts both stiffening and softening frequency responses for the inter-well and intra-well oscillations of bi-stable systems. Preliminary meso-scale experiments match well with the dynamic simulation and show that the softening frequency response generates much higher power than mono-stable configuration at lower frequencies, providing opportunity for MEMS harvesters to be operated at low frequency and low g input vibrations. MEMS-scale multi-layer buckled plate test results show that at least 50 μW power could be generated below 100 Hz frequency and 0.2 g acceleration (Figure 22).

Prior studies have shown that the presence of nonlinearity based on magnetic interaction or buckled beams has a significant influence on the performance of energy harvesters. The bandwidth of nonlinear energy harvester was increased by bistable effect, however, it is obvious that the frequency response to input vibration was more complicated as compared to linear case. The instability of

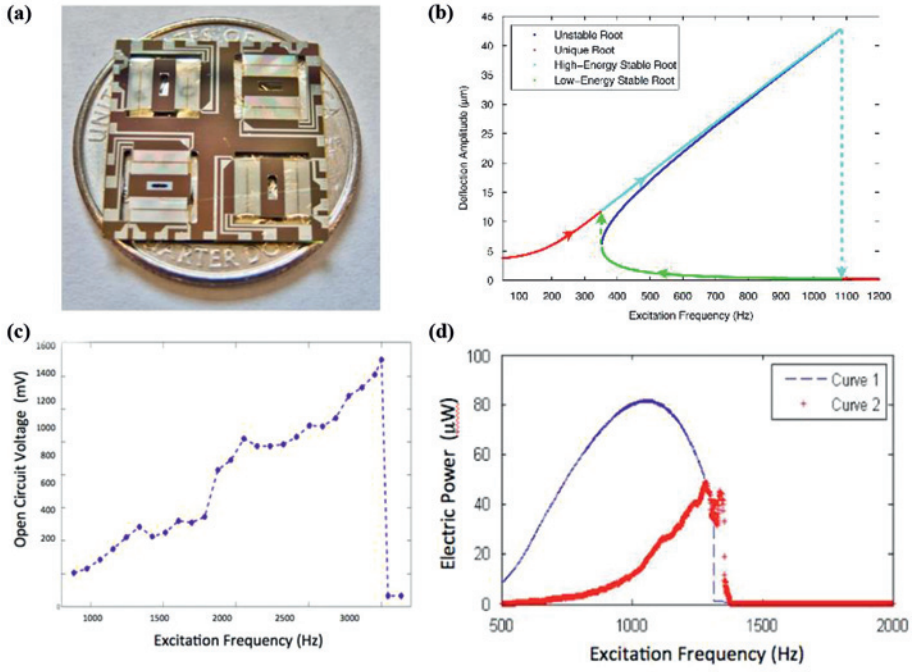

Figure 21: Non-linear beam MEMS energy harvester with ultra-wide bandwidth (a) Photo of fabricated device on a coin. (b) Simulated dynamic response of a nonlinear resonator. (c) Open circuit voltage versus frequency (note that nonlinear stretching happens twice in each excitation cycle). (d) Curve 1: estimated extractable power versus frequency, Curve 2: Generated power via the piezoelectrics (Hajati and Kim 2011).

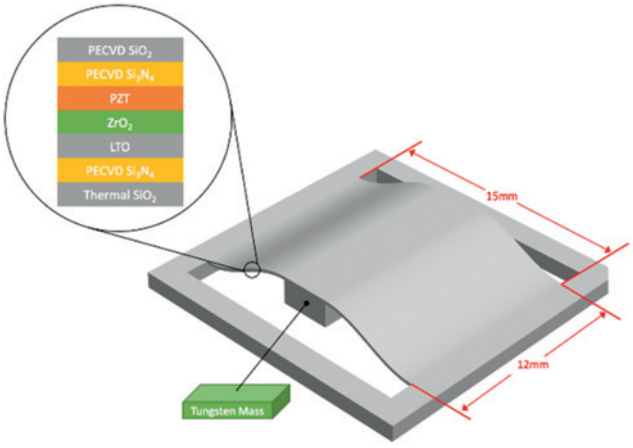

Figure 22: Schematic view of a bi-stable beam energy harvester (Xu and Kim 2015).

frequency response makes it difficult to precisely modulate the bandwidth and tune the resonance frequency of the energy harvester in realistic environment. We expect that nonlinearity can provide a solution for widening the bandwidth but it will require additional control features to exploit the enhancement in the output power.

3.6 Self-resonance Frequency Tuning Technique

To maximize output power, energy harvesters should be excited in resonance with external vibration sources. In the other words, the natural frequency of the energy harvester should be matched to those of external vibration sources. The typical linear energy harvester has only one dominant natural frequency which should be carefully selected in accordance with the external vibration frequency. However, when the excitation frequency is unknown or varies with time, the energy harvester with fixed natural frequency cannot achieve an optimal output power. Therefore, in practice, the resonance frequency tuning scheme is essential to increase its power output. Most reported frequency tuning mechanisms are passively adjusted or require additional energy in order to automatically tune the frequency. Hence, the self-frequency tuning mechanisms which do not require extra energy or very small amount energy for autonomous tuning are necessary.

Jo et al. presented the cantilever structure that can automatically switch its natural frequency and maintain

its switched frequency without an additional energy consumption (Jo, Kim, and Kim 2011). The proposed harvester was composed of a cantilever couple with different lengths, similar to seesaw structure. The coupled cantilevers are able to move laterally and have two different optimal vibration phases at each resonance frequencies. As shown in Figure 23, the vibration phase of the coupled energy harvesters can shift to the other phase when the external frequency are closed to the resonance frequency of the other phase. The difference between the horizontal inertia forces by deflection difference of cantilevers is the key to switch the harvester between the two phases. This harvester is self-frequency tunable and no additional power is required for tuning. As shown in Figure 24, this harvester cannot cover whole frequency range but still is much more efficient than typical harvesters.

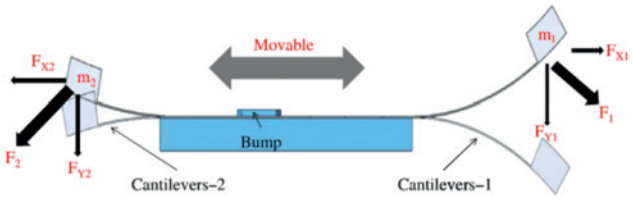

Figure 23: Schematic view of resonance frequency switchable energy harvester (Jo, Kim, and Kim 2011).

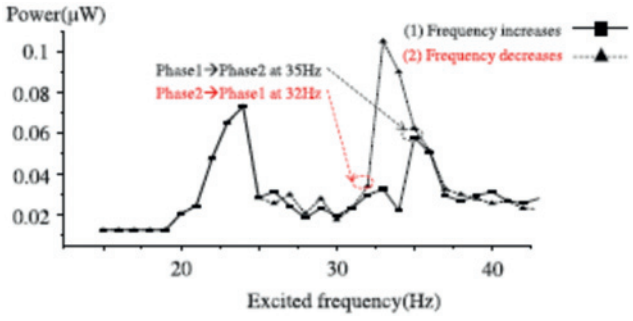

Figure 24: Output power of frequency switching scheme: (1) when the excited frequency increases from 10 Hz, the first output peak shows at 24 Hz and the second peak shows at 35 Hz, (2) when the excited frequency decreases from 40 Hz, the first output peak shows at 33 Hz and the second peak shows at 24 Hz (Jo, Kim, and Kim 2011).

The close loop active frequency tuning system have been proposed by Zhu et al. (2008). The schematic of tuning mechanism is described in Figure 25. The natural frequency of energy harvester can be adjusted by attraction force between two magnets. The magnetic force also can be controlled by changing distance of two magnets using the linear actuator. Thus, the axial load on the cantilever can be changed. Overall tuning process was controlled by a microcontroller which detects the output voltage of the generator periodically and gives an instruction to drive a linear actuator to adjust the distance between two magnets. When the output power reaches maximum, the system changes to sleep mode to save power. The microcontroller periodically wakes up to monitor the power output and execute natural frequency tuning process. They claimed that the microcontroller and linear actuator can be operated using only power generated from microgenerator itself. However, the power consumption for frequency tuning procedure was still very high on the order of 2.04 mJ/mm. If one can dramatically reduce the power consumption of the microcontroller and linear actuator, the closed loop frequency tuning system could be one of the promising candidate for self-resonance tuning technique except in continuously varied frequency or complex mode vibration environment.

3.7 Low Frequency Energy Harvesting Structures

Micro scale low frequency energy harvester has been mainly dominated by inductive or electromagnetic devices. However, the miniaturization of such devices is limited by the size of the magnet used as the inertial mass and the size of the coil that can be fabricated on the MEMS scale. Consequently, for MEMS scale energy harvester, piezoelectricity is the transduction of choice and especially due to its compatibility with cleanroom based silicon micromachining techniques. Recent study by Mitcheson et al. (2007) has shown that at mm-scale, piezoelectric mechanism provides the best output power density at low frequencies as compared to other possible mechanisms for vibration EH. However, piezoelectric based energy harvester presents a fundamental challenge at the small dimensions since the resonance frequency of the structure increases (kHz range) as the dimension decreases. This challenge should be overcome in order to become compatible with the practical applications.

The most commonly used approach for reducing the natural frequency involves the addition of a large inertial tip mass to the free end of a simple single cantilever beam structures (Choi et al. 2006; Liu et al. 2012; Tsujiura et al. 2013; Xu et al. 2012a). Other methods involve the use of increased effective surface area cantilevers such as spirals (Deterre et al. 2013). Recently, Song et al. demonstrated the spiral MEMS energy harvesters using typical silicon

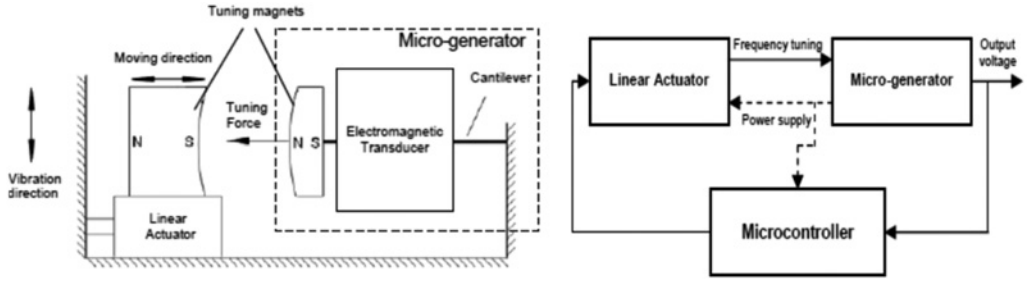

Figure 25: Schematic diagram of the closed loop tuning system (Zhu et al. 2008).

MEMS process as shown in Figure 26. In order to understand the natural frequency characteristics of the spiral cantilever structure, different turns of spiral MEMS harvesters were fabricated as illustrated in Figure 26(b). The natural frequency of the spiral MEMS harvester was inversely proportional to number of turns and can be reduced to less than 50 Hz within 1.85 mm diameter circle active dimension. The generated output voltage was gradually increased until 5 turns and then started to slightly decrease with increasing number of turns. This might be because the active dimension of spiral region was gradually increased and thus voltage cancelation mode due to torsion are more likely to dominate with higher number of turns. Five turn spiral energy harvester showed the maximum generated voltage. More precise MEMS fabrication process and structural modification to reduce the complex vibration modes are required in producing higher turn spiral energy harvesters.

The use of tip masses severely affects the structural integrity and durability of the harvesters while the increased effective surface area designs exhibit torsion (causing voltage cancellation effect) in the very important first vibration mode. Therefore, it is of great importance to create a more effective method by developing uniquely

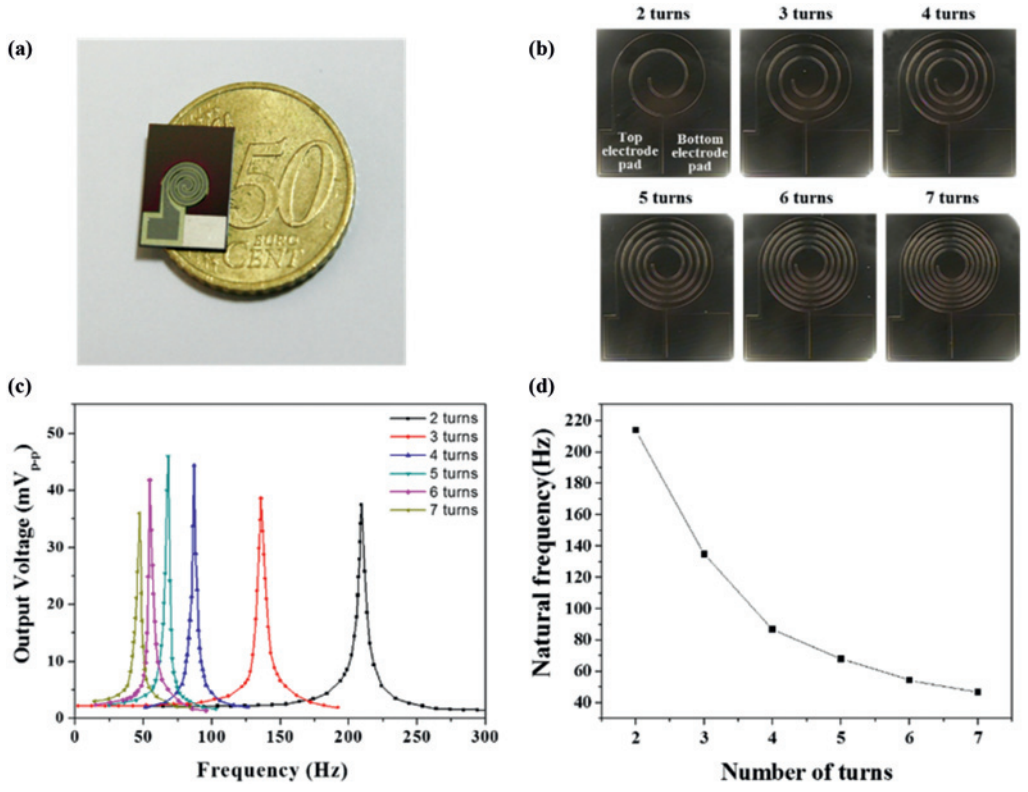

Figure 26: (a) Spiral MEMS energy harvester with low natural frequency (a) photo of fabricated device on a coin, (b) spiral MEMS energy harvesters with variation of number of turns, (c) open circuit output voltage versus frequency with number of turns of spiral MEMS energy harvesters, and (d) natural frequency variation with number of turns.

shaped cantilevers, such as arc-based cantilevers, which exhibit low natural frequencies. To harvest energy at the low frequency of ambient vibrations, extensive research has led us to the development of circular Zigzag structure that permits inertial mass free attainment of such low frequencies. Recently, Varghese et al. reported a set of new tip mass free vibration energy structures that are capable of attaining resonant frequency of less than 100 Hz with less torsion than spiral designs and with a smaller foot print than zigzag or meandering structures, as shown in Figure 27 (Apo 2014; Varghese 2013). This design, termed as arc-based cantilever (ABC), has achieved <100 Hz resonant operation both on the Si MEMS platform and with bulk piezo material as compared to traditional cantilevers. The arc-based cantilever is a continuous cantilever that can be divided into purely circular arc segments, thereby making it a low frequency structure with dominant bending characteristic in the first (or fundamental) frequency mode (Apo, Sanghadasa, and Priya 2013). Different configurations of micro ABCs were investigated through analytical modeling and validation experiments. As shown in Figure 27(a), two arc-based micro-cantilevers (S-shaped, C-shaped) were designed based on the well-known linear configurations (simple and zigzag.) In addition to the metal micromilling, [Figure 27(b)] such structures were also fabricated and demonstrated using a silicon micromachining process [Figure 27(c)]. All the arc-based cantilevers were shown to resonate below 100 Hz and they exhibited dominant bending behavior in the fundamental mode (Apo, Sanghadasa, and Priya 2013, 2014). These designs therefore provide a foundation for the development of standalone arc-based micro-cantilevers which can be used for energy harvesting, actuation and sensing applications. The model for ABC structures is based on the classical Timoshenko beam theory and includes the effects of bending, torsion, transverse shear deformation and rotary inertia. It was developed with a provision for multilayered beam modeling (Apo 2014). The micro-cantilever can be modified and optimized to fit desired configurations based on the numbers of arcs, longest side length, spacing and width.

Recently, Sharpes et al. also demonstrated a strategy of using highly compliant two-dimensional beam shapes to harvest energy from low frequency excitations (Sharpes, Abdelkefi, and Priya 2015). They fabricated 3 different 2D shapes of Zigzag, Flex and Elephant configurations as shown in insets of Figure 28(a), (b) and (c). All of samples occupy a $25.4 \times 25.4\,mm^2$ (1 $inch^2$) area and fabricated using mild steel and APC850 piezoelectric ceramics. In order to maintain the low natural frequency, the piezoelectric layers were placed at the most stress concentrated single area of each shapes rather than whole area through a finite element simulation. Neodymium magnet tip masses of 1.88 g weight were attached to the end of each beams to decrease resonance frequency and increase out power. As shown in Figure 28(a), the Zigzag harvester is capable of producing 2.93 μW across 0.75 MΩ at 65.6 Hz. The Flex harvester produced 32.2 μW across 1 MΩ at 62.0 Hz base

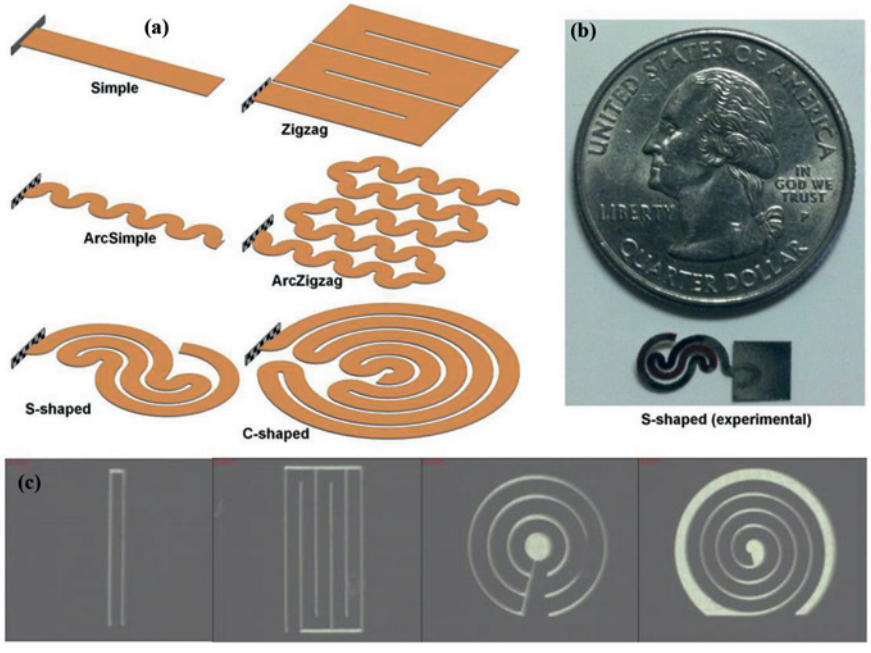

Figure 27: Arc-based microcantilvers: (a) Design development of the cantilevers, (b) Micromilled S-shaped cantilevers (Apo 2014), (c) As fabricated silicon MEMS cantilever structures (Varghese 2013).

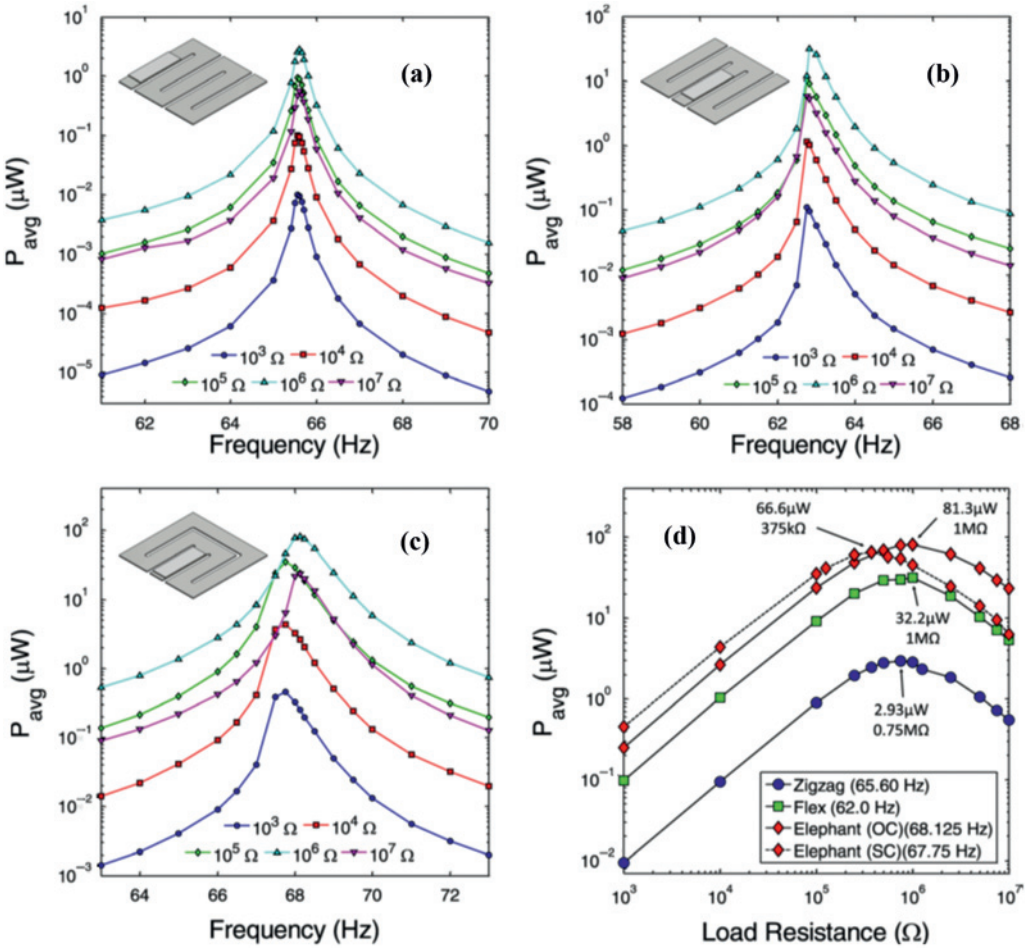

Figure 28: Experimental results for average power production as a function of frequency and electrical load resistance for (a) Zigzag, (b) Flex, and (c) Elephant configurations, with (d) Average power as a function of electrical load resistance at each harvester's respective resonance frequency. All input vibrations were at 0.1 g base acceleration (Sharpes, Abdelkefi, and Priya 2015).

excitation frequency in Figure 28(b). In both designs, the electromechanical coupling is quite small, as no frequency shift was observable between the short-circuit ($R_L = 10^3\,\Omega$) and open-circuit ($R_L = 10^7\,\Omega$) frequencies. However, for the Elephant harvester, we note a substantial shift between short-circuit and open-circuit frequencies, as well as, a large power output of 81.3 μW across 1 M Ω at 68.125 Hz, as shown in Figure 28(c). From these findings, we can conclude the merits of Elephant design, and how it is beneficial towards efficient low-frequency piezoelectric energy harvesting compared to the other shapes.

Two main issues in realizing MEMS energy harvesters are the broadband and low operational resonance frequency. Previously discussed low resonance frequency structures with nonlinear behavior excited through the magnetic coupling or the buckled structure could provide breakthrough. In addition to design of nonlinear broadband vibration structure for low resonance frequency, the MEMS fabrication process for incorporating complex structures should be developed.

3.8 Development of New Fabrication and Characterization Methodologies

Unlike inductive harvesting, piezoelectric and magnetoelectric devices lend easily to MEMS scaling. The processing of such Piezo-MEMS devices often requires special fabrication, characterization and testing techniques. Generally, MEMS devices are fabricated on silicon wafer starting with growth of high quality piezoelectric films. Ron et al. developed a novel fabrication methodology to realize these structures with reduced number of

processing steps (Varghese 2013). They also described the extensive work on MEMS wafer test bench setup.

The MEMS fabrication process flow consisted of two modules as shown in Figure 29: (a) the electrical module for PZT capacitor formation and (b) the mechanical module wherein the Si based micro-cantilever structures were created (Varghese 2013). When the modules are combined, this simplified process flow reduces the number of fabrication steps by ~40 %. Using this modular approach, a self-aligned and self-isolated MEMS fabrication process with only two photolithography steps was demonstrated, as shown in Figure 29(c). The key feature of this process is the use of a patterned SiO_2 hard mask to define the beam thickness in the DRIE and then after removal of that SiO_2 hard mask, using a 2nd patterned photoresist mask to proceed with a 2nd DRIE to release the cantilever. Unlike the process used for the unreleased MEMS structure of a Piezo accelerometer (Durou et al. 2010), this process is developed to a) in-situ remove the SiO_2 hard mask before the 2nd DRIE and b) then conduct the 2nd DRIE on the front side for release. The removal of the SiO_2 hard mask after the 1st DRIE can be skipped in some cases and the DRIE SiO_2:Si etch rate selectivity can be utilized to define the cantilever beam thickness. That is, after SiO_2 hard mask definition, 1st DRIE and 2nd DRIE mask pattern is applied, but SiO_2 need not be removed. This inorganic hard mask will etch slower than Si and thus when the Si DRIE reaches the front of the wafer, the sections that were covered by SiO_2 would have lagged behind during etch and would be thicker. Using this modular approach, different cantilever structural designs were investigated and based on this learning, a low frequency structure that resembles an arc-based cantilever was developed [Figure 29(c)].

For electrical testing, MEMS harvesters are generally tested individually after the wafer has been singulated by dicing. This requires that the MEMS device be packaged or temporarily glued to a special carrier wafer without damage. Prior to packaging and simulation, Ron et al. introduced a novel concept of wafer level testing (Varghese 2013). As shown in Figure 30(a), wafer probe card is fabricated from a custom printed circuit board (PCB) with gold plated pogo pin probes, where all the pogo pin locations and wiring were designed according to the MEMS device layout on the wafer. All wiring is thus confined to the outside of the test setup and does not

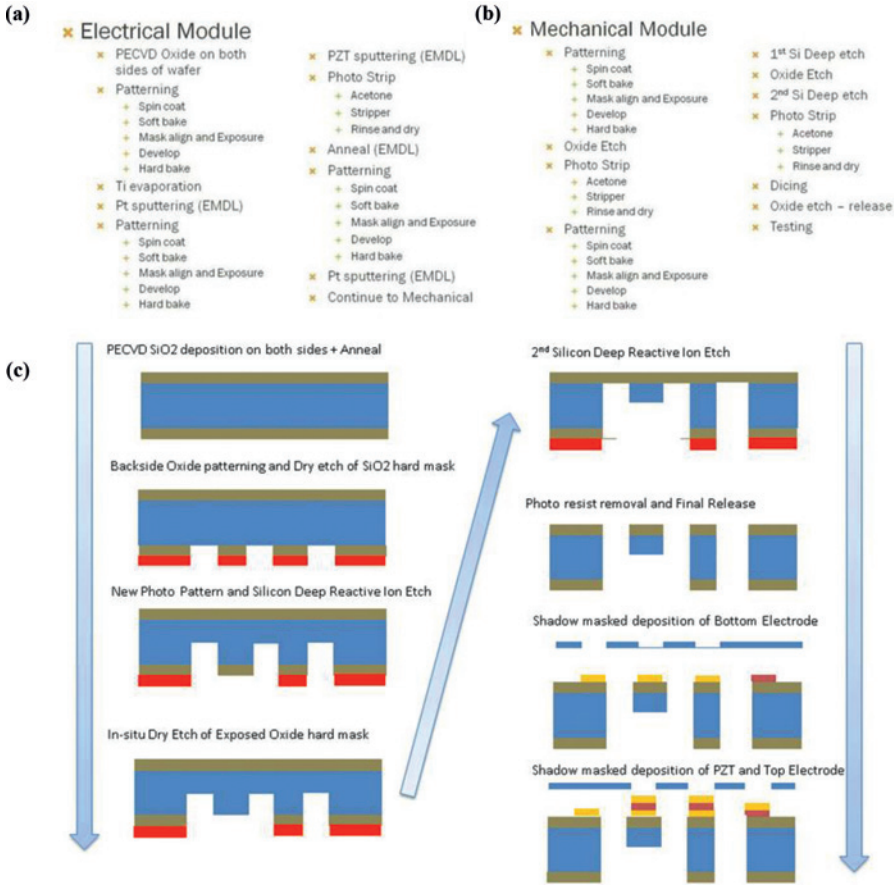

Figure 29: Fabrication process details of the modules in a Piezo-MEMS process flow (a) Electrical module, (b) Mechanical module, and (c) Schematic of the MEMS fabrication process with two lithography steps (Varghese 2013).

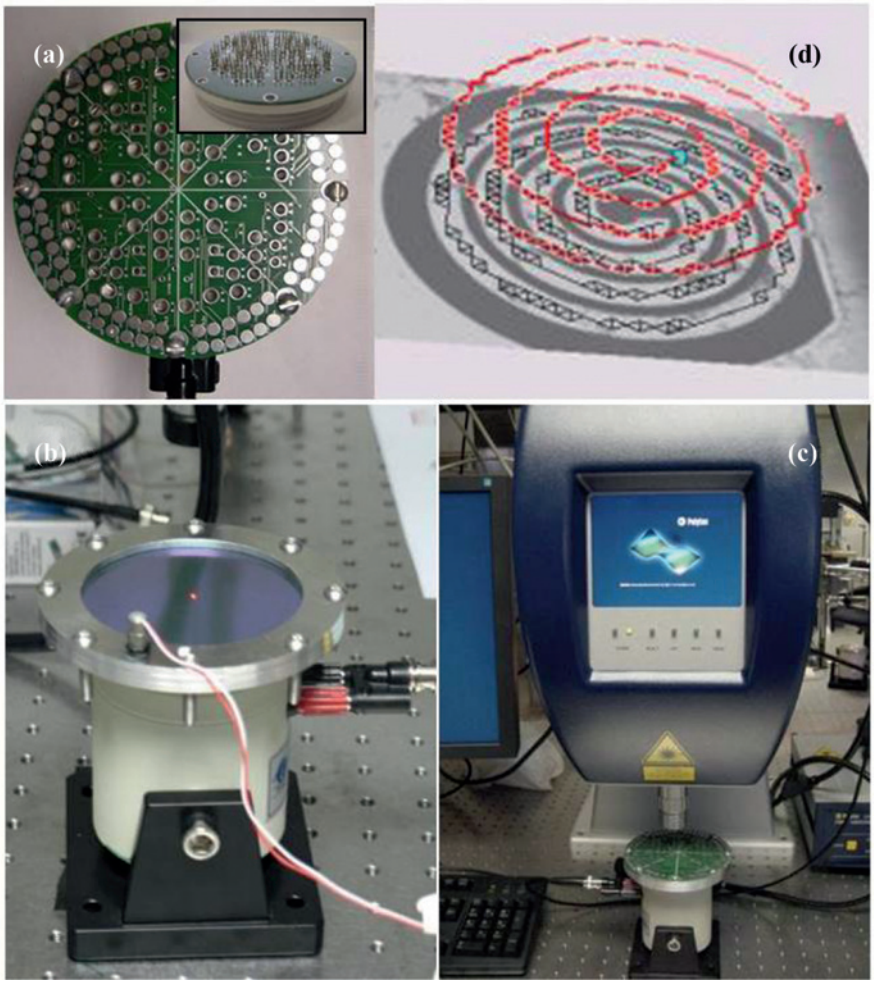

Figure 30: (a) As manufactured PCB board with pogo pins soldered on and (b) Clamped over a device wafer, (c) Vibration measurement setup with 3D laser vibrometer, (d) Animation plots of the velocity FRF at fundamental resonance of a arc-based micro cantilever (Varghese. 2013).

interfere with the laser vibrometry measurement [Figure 30(b)]. For mechanical testing of MEMS wafers, a Polytec MSA 500 was used with a special clamp that holds the wafer along its edges, as shown in Figure 30(c). As the shaker is moving, the whole wafer and all its MEMS devices move simultaneously, thus, one can scan each cantilever from tip to base and take the transfer function between the tip and base to compute the resonance frequency. Typical 3D animation plot of the actual vibration characteristics is illustrated in Figure 30(d). This approach is especially useful if one has numerous devices on a wafer.

4 Circuit for Impedance Matching

Maximum power transfer occurs when the load impedance is the complex conjugate of the source impedance. Since a piezoelectric generator exhibits a large capacitive term as shown in Figure 31, a complex conjugate matching requires a large inductance for the load to cancel the capacitive term. For example, the required inductance is 137 H at 44 Hz for the piezoelectric generator in Figure 31 and 470 H at 50 Hz. Further, the inductance value depends on the vibration frequency. Therefore, it is impractical to use a passive inductor for the matching. Saggini et al. investigated a complex conjugate matching scheme, which emulates an inductor (Saggini et al. 2010). They used a bidirectional DC/DC converter, in which the input voltage is higher than the output voltage. So the current flows from the piezoelectric generator to the battery under the buck mode and in the opposite direction under the boost mode. Their approach results in a complex circuit to dissipate large power. An alternative solution to the complex conjugate matching is to adopt resistive matching. Suppose that the source impedance of a piezoelectric generator $Z_s = R_S + jX_S$ is connected in

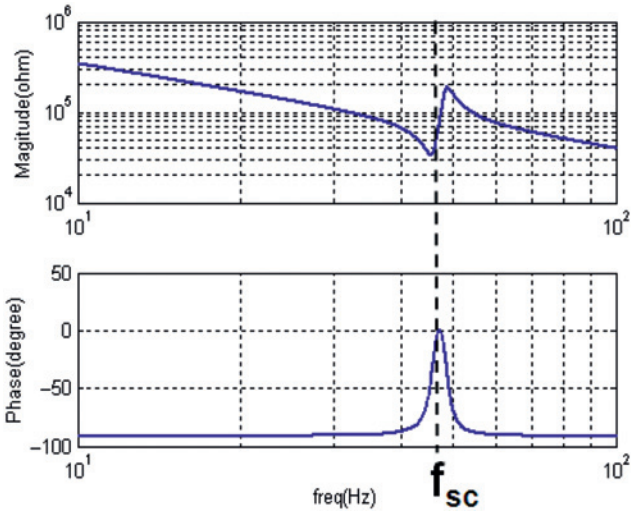

Figure 31: Magnitude and phase of a PZT cantilever.

series with the load resistance R_L. The optimal value of R_L for the maximum power transfer is expressed as: $R_L = \sqrt{R_S^2 + X_S^2}$ (Kong et al. 2010). Note that the optimal R_L is a function of R_S and X_S, i. e., dependent on the excitation frequency of the piezoelectric generator. Hence, it requires a harvester circuit to change the load resistance value dynamically according to the excitation frequency, and the operation is called maximum power point tracking (MPPT). The cost for a resistive matching compared with a complex conjugate matching is that the maximum power is delivered to the load only at the resonant frequency. The power level drops sharply at frequencies away from the resonant frequency (Kong and Ha 2012).

4.1 Maximum Power Point Tracking for PZT Resistive Matching

The source impedance of a transducer such as piezoelectric generator and photovoltaic cell changes as the operating condition changes, which requires MPPT. Deployment of an MPPT scheme is advantageous only when the additional power harvested owing to the MPPT is greater than the power dissipated by the MPPT circuit itself. As the additional power, which can be harvested through the MPPT, is limited by the transducer and its operating condition, there exists a breakeven point for adoption of an MPPT scheme. Another design issue with MPPT is accuracy and speed of the tracking, which are often traded. Also, a more accurate and hence more sophisticated MPPT scheme dissipates more power for the MPPT circuit. So adoption of an accurate scheme does not necessarily increase the net energy harvested.

Two commonly adopted MPPT algorithms for energy harvesting are hill climbing and fractional open circuit voltage (FOCV). The hill climbing algorithm, also called "perturb and observe", for the dynamic resistive matching is illustrated in Figure 32. It increments the load resistance by a predetermined step and then measures the power, often the average current, delivered to the load. If the power increases, the search direction is correct, and it increments the resistance again in the next cycle. If the power decreases, it reverses the direction. The algorithm guarantees convergence to the optimal point if there is no local maxima, and it is the case for piezoelectric generators. The hill climbing algorithm can be implemented with a microcontroller unit (MCU) or a mixed-signal circuit (Kong, Deyerle, Ha, 2011; Sankman and Ma 2014). Considering the voltage of a storage device roughly remains the same for each cycle, the power can be measured through measurement of the average current into the storage device. The FOCV algorithm relies on the fact that the voltage across the load is one half of the open circuit voltage of the source (Lu, Tsui, and Ki 2011, Shim et al. 2015). The FOCV algorithm is simpler to implement compared with the hill climbing algorithm. However, the FOCV algorithm necessitates the load be open once in a while to measure the open circuit voltage, and the energy harvesting is interrupted during the time.

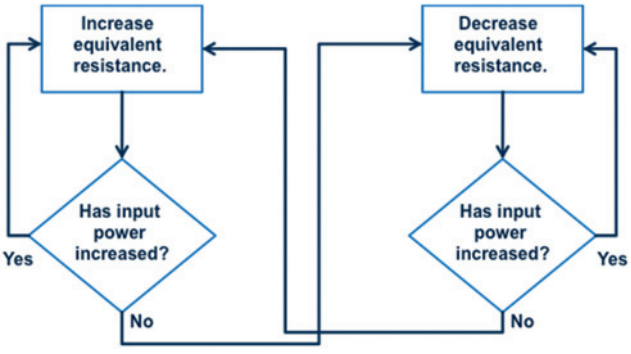

Figure 32: Schematic description of the Hill climbing algorithm.

As noted earlier, the optimal load resistance for a resistive matching for a piezoelectric generator is $R_L = \sqrt{R_s^2 + X_s^2}$ The load resistance seen by the piezoelectric generator is the input resistance of the converter connected to the generator. The effective input resistance of a buck-boost converter in the discontinuous conduction mode (DCM) is obtained as $R_{in} = \frac{2L}{D^2 T_s}$, where L is the inductance, D is the duty cycle, and T_S is the switching

period. So the duty cycle D can be controlled to change the effective input resistance of the converter. It should be noted that the duty cycle D is changed to control the input resistance, and the output voltage of the converter is also changed accordingly. To regulate the output voltage, it needs another converter stage or some other means such as use of a Zener diode.

Once MPPT achieves the optimal or near optimal resistor value, the MPPT operation can be halted to save power until the operation condition changes. A design issue is to set the optimal wake up and sleep periods or duty cycle, which depends on several factors such as the speed and amount of the operating condition change and the speed of MPPT.

4.2 Synchronized Switch Harvesting on Inductor (SSHI) and Synchronous Electric Charge Extraction (SECE)

Synchronized Switch Harvesting on Inductor (SSHI) aims to eliminate the effect of the capacitive term of piezoelectric generators (Guyomar et al. 2005; Ramadass and Chandrakasan 2010, Wu et al. to appear). Figure 33 shows an SSHI circuit composed of an inductor L and a switch S. Note that the PZT model in the figure is a simplified Norton equivalent circuit. The PZT capacitor C_p is negatively charged at the crossing point of the PZT current I_p from negative to positive. The SSHI scheme minimizes the wasted energy to charge the capacitor positively using an LC resonant circuit. The switch SW is closed momentarily right after the zero crossing of the PZT current i_p. The capacitor C_p and the inductor L form a resonant circuit with a resonant frequency much higher than the PZT vibration frequency. The capacitor voltage V_P rises quickly due to the oscillation of the resonant circuit, and then the switch is opened at the opposite peak value of V_P, reducing dispense of the PZT energy to discharge the capacitor. When PZT current I_p changes from positive to negative, the same operation is performed to save the energy for charging the capacitor negatively. An SSHI circuit increases the energy harvested when compared with a rectifier only circuit at the cost of higher circuit complexity.

The SSHI scheme requires impedance matching for maximum power transfer. Synchronous Electric Charge Extraction (SECE), which is an extension of the SSHI method, eliminates such a need. The SECE scheme uses an LC resonant circuit to transfer the energy stored in the PZT capacitor to the inductor first and then the inductor energy is transferred to the load through a DC-DC converter (Lefeuvre et al. 2005, Gasnier et al. 2014, and Dini et al. 2016). The extracted power of the SECE method does not depend on the load, and so the load can vary without affecting the efficiency.

4.3 Rectifiers and Voltage Doublers

Piezoelectric generators require rectification in order to convert output AC voltage in to DC. A full bride rectifier with passive diodes can be easily incorporated but the forward diode voltage drop can cause substantial power loss. Active or synchronous rectifiers reduce losses associated with passive diodes. An active rectifier turns on or off a MOSFET in appropriate time periods to effectively rectify the voltage (Hashemi, Sawan, and Savaria 2012; Lam, Ki, and Tsui 2006; Le et al. 2006). Figure 34 shows a comparator based active rectification, which senses the polarity of the input voltage to turn on or off the MOSFET. If the current through the MOSFET is small, e. g. near crossing zero points, the difference in the drain and source voltage is small to cause an operation error. Various circuit configurations for rectifications have been suggested (Rincón-Mora and Yang, 2016; Hwang et al. 2015), and a major design issue is to lower power dissipation of the gate control circuit, such as the comparator shown in Figure 34. Another issue with piezoelectric generator is that the rectified voltage is very small, which leads to low efficiency of the boost converter. A voltage doubler can be used to mitigate this issue (Tabesh and Fréchette 2010).

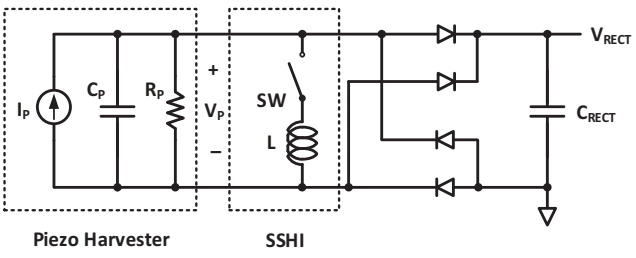

Figure 33: Synchronized Switch Harvesting on Inductor (SSHI).

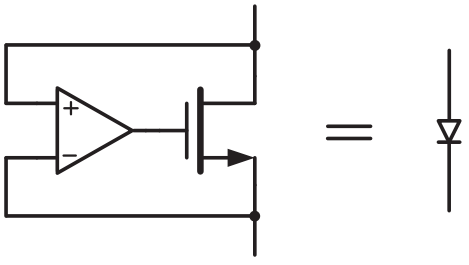

Figure 34: Circuit diagram for active rectification.

A voltage doubler increases the output voltage by 2X while rectification. It is possible to combine the voltage doubling technique and active diodes.

Recently, reconfigurable power management circuit using a 0.25 µm complementary metal-oxide semiconductor (CMOS) process has been developed by KAIST and SNU team (Hwang et al. 2015) as shown in Figure 35. The multiple storage capacitors of the reconfigurable charger array can adjust the magnitude of capacitance by controlling serial and parallel alignments of capacitors. At the charging stage, impedance is matched between the reconfigurable capacitor array and the energy harvester to extract maximum energy while minimizing energy loss, whereas at the discharging stage, the capacitors are rearranged to supply the demanded constant low-voltage into the external load. The reconfigurable rectifying circuit can transfer four times higher electric energy to the load resistor compared to the traditional rectifying circuit.

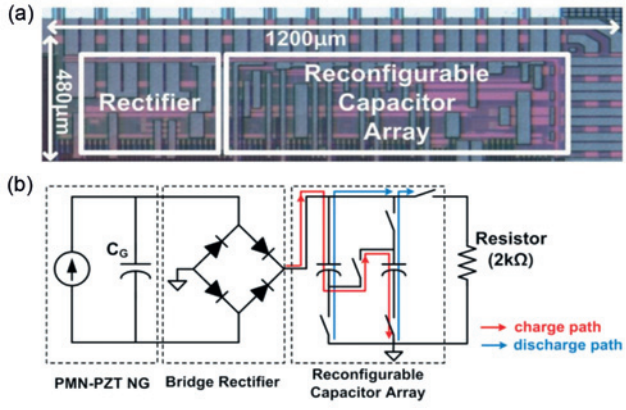

Figure 35: (a) A top-view optical microscopy image and (b) schematic circuit diagram of the reconfigurable rectifying circuit system integrated with energy harvester, bridge rectifier, reconfigurable capacitor charger array, and external load. (Hwang et al., 2015)

5 Summary

MEMS piezoelectric energy harvesters at the ~mm^3 dimensions will lead to battery-less autonomous sensors systems and networks if 10's to 100's µW of power can be extracted from the ambient vibration continuously, robustly and at low cost. The key attributes to make a good piezoelectric MEMS energy harvester can be summarized as its compactness, output voltage, output power (density), bandwidth, operating frequency, input vibration amplitude, lifetime and cost. Among them, higher power density and wider bandwidth of resonance are the two biggest challenges currently facing the technology. Figure 36(a) and (b) and Table 1 show the normalized power densities of some recently developed MEMS energy harvesters, where orders of magnitude improvement can be seen in the last 5 years. Giant piezoelectric coefficient materials, epitaxially grown films, grain textured piezoelectric materials and thin/thick films, high performance lead-free piezoelectric materials are the recent advancements made towards increasing the electromechanical energy conversion of piezoelectric harvesters. Nonlinear resonators are extremely promising to extract more electrical energy from the beam. Recent advances in piezoelectric materials and harvester structural design, individually or in combination, are bringing us closer to battery-less autonomous sensors systems and networks. We expect that in the near future, a coin size harvester will be able to harvest about 100µW continuous power below 100 Hz at less than 0.5 g vibration and at reasonable cost. High efficiency and low power dissipation of energy harvester circuits will

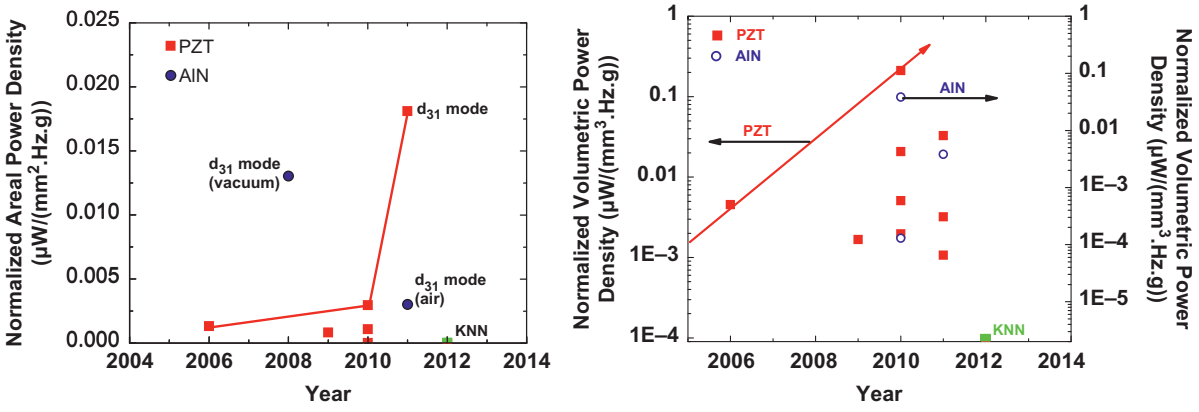

Figure 36: Normalized (a) areal (µW/(mm^2.Hz.g)) and (b) volumetric power density (µW/(mm^3.Hz.g)), of piezoelectric MEMS energy harvesters recently reported in Table 1.

remain important and be critical to maximize the net energy harvested for future micro-scale energy harvesters.

Funding: H.-C.S. and A.C. acknowledges the support from Office of Basic Energy Sciences, Department of Energy (DE-FG02-06ER46290), Y.Z. and R.V. acknowledge support from AFOSR (FA9550-14-1-0376), S.-G.K. acknowledges the support from DARPA Grant (HR0011-06-1-0045), MIT-Iberian Nanotechnology Laboratory Program. Works at KIMS were supported by KIMS internal R&D programs (PNK4661 and PNK4991). Dong Ha's work was supported in part by the Center for Integrated Smart Sensors funded by the Korea Ministry of Science, ICT & Future Planning as Global Frontier Project (CISS-2-3). S.P. acknowledges the financial support from Norfolk State University through NSF CREST program.

References

Ahn, C.-W., C.-H. Choi, H.-Y. Park, S. Nahm, and S. Priya. 2008a. "Dielectric and Piezoelectric Properties of $(1-x)(Na_{0.5}K_{0.5})NbO_3$–$xBaTiO_3$ Ceramics." *Journal of Materials Science* 43:6784–97.

Ahn, C.-W., D. Maurya, C.-S. Park, S. Nahm, and S. Priya. 2009. "A Generalized Rule for Large Piezoelectric Response in Perovskite Oxide Ceramics and Its Application for Design of Lead-Free Compositions." *Journal of Applied Physics* 105:114108.

Ahn, C.-W., C.-S. Park, D. Viehland, S. Nahm, D.-H. Kang, K.-S. Bae, and S. Priya. 2008b. "Correlation Between Phase Transitions and Piezoelectric Properties in Lead-Free (K, Na, Li) NbO_3–$BaTiO_3$ Ceramics." *Japanese Journal of Applied Physics* 47:8880.

Aita, C. 1982. "Basal Orientation Aluminum Nitride Grown at Low Temperature by RF Diode Sputtering." *Journal of Applied Physics* 53:1807–8.

Akedo, J., and M. Lebedev. 2000. "Piezoelectric Properties and Poling Effect of Pb (Zr, Ti) O_3 Thick Films Prepared for Microactuators by Aerosol Deposition." *Applied Physics Letters* 77:1710.

Aktakka, E. E. 2012. "Integration of Bulk Piezoelectric Materials into Microsystems." Ph. D Dissertation in the University of Michigan.

Al-Ashtari, W., M. Hunstig, T. Hemsel, and W. Sextro. 2012. "Frequency Tuning of Piezoelectric Energy Harvesters by Magnetic Force." *Smart Materials and Structures* 21:035019.

Ando, B., S. Baglio, C. Trigona, N. Dumas, L. Latorre, and P. Nouet. 2010. "Nonlinear Mechanism in MEMS Devices for Energy Harvesting Applications." *Journal of Micromechanics and Microengineering* 20:125020.

Andosca, R. A., T. G. McDonald, V. Genova, S. Rosenberg, J. Keating, C. Benedixen, and J. Wu. 2012. "Experimental and Theoretical Studies on MEMS Piezoelectric Vibrational Energy Harvesters with Mass Loading." *Sensors and Actuators A: Physical* 178:76–87.

Apo, D. J. 2014. "Low Frequency Microscale Energy Harvesting." Ph. D. Disseration in Virginia Tech.

Apo, D. J., M. Sanghadasa, and S. Priya. 2013. "Low Frequency ARC-based MEMS Structures for Vibration Energy Harvesting." Paper presented at the 8th IEEE International Conference on Nano/Micro Engineered and Molecular Systems, 615–8.

Apo, D. J., M. Sanghadasa, and S. Priya. 2014. "Vibration Modeling of Arc-Based Cantilevers for Energy Harvesting Applications." *Energy Harvesting and Systems* 1:57–68.

Baek, S., J. Park, D. Kim, V. Aksyuk, R. Das, S. Bu, D. Felker, J. Lettieri, V. Vaithyanathan, and S. Bharadwaja. 2011. "Giant Piezoelectricity on Si for Hyperactive MEMS." *Science* 334: 958–61.

Barton, D. A., S. G. Burrow, and L. R. Clare. 2010. "Energy Harvesting From Vibrations with a Nonlinear Oscillator." *Journal of Vibration and Acoustics* 132:021009.

Bayraktar, M., A. Chopra, F. Bijkerk, and G. Rijnders. 2014. "Nanosheet Controlled Epitaxial Growth of PbZr0.52ti0.48O3 Thin Films on Glass Substrates." *Applied Physics Letters* 105:132904.

Bedekar, V., J. Oliver, and S. Priya. 2010. "Design and Fabrication of Bimorph Transducer for Optimal Vibration Energy Harvesting." *IEEE Transactions on Ultrasonics, Ferroelectrics, and Frequency Control* 57:1513–23.

Beeby, S. P., M. J. Tudor, and N. White. 2006. "Energy Harvesting Vibration Sources for Microsystems Applications." *Measurement Science and Technology* 17:R175.

Bernstein, J., J. Bottari, K. Houston, G. Kirkos, R. Miller, B. Xu, Y. Ye, and L. Cross. 1999. "Advanced MEMS Ferroelectric Ultrasound 2D Arrays." Paper Presented at the IEEE Ultrasonics Symposium, 1145–53.

Bertacchini, A., S. Scorcioni, D. Dondi, L. Larcher, P. Pavan, M. Todaro, A. Campa, G. Caretto, S. Petroni, and A. Passaseo. 2011. "AlN-based MEMS Devices for Vibrational Energy Harvesting Applications." Paper Presented at the European Solid-State Device Research Conference, 119–22.

Bono, D. C., A. Sliski, J. Huang, and R. C. O'handley. 2009. "High Efficiency, Inductive Vibration Energy Harvester." US Patent 7,569,952.

Brennecka, G. L., W. Huebner, B. A. Tuttle, and P. G. Clem. 2004. "Use of Stress to Produce Highly Oriented Tetragonal Lead Zirconate Titanate (PZT 40/60) Thin Films and Resulting Electrical Properties." *Journal of the American Ceramic Society* 87:1459–65.

Chandrakasan, A., R. Amirtharajah, J. Goodman, and W. Rabiner. 1998. "Trends in Low Power Digital Signal Processing." Paper Presented at the IEEE International Symposium on Circuits and Systems, 604–7.

Chen, S. Y., and I. W. Chen. 1994. "Temperature–Time Texture Transition of Pb $(Zr_{1-x}Ti_x)O_3$ Thin Films: I, Role of Pb-Rich Intermediate Phases." *Journal of the American Ceramic Society* 77:2332–6.

Choi, W., Y. Jeon, J.-H. Jeong, R. Sood, and S.-G. Kim. 2006. "Energy Harvesting MEMS Device Based on Thin Film Piezoelectric Cantilevers." *Journal of Electroceramics* 17: 543–8.

Chopra, A., M. Alexe, and D. Hesse. 2015a. "Fabrication and Orientation Control of Highly Cation-Ordered Epitaxial

$PbSc_{0.5}ta_{0.5}O_3$ Thin Films on Si (100." *Journal of Applied Physics* 117:044102.

Chopra, A., M. Bayraktar, F. Bijkerk, and G. Rijnders. 2015b. "Controlled Growth of $PbZr_{0.52}ti_{0.48}O_3$ Using Nanosheet Coated Si (001." *Thin Solid Films* 589:13–16.

Chopra, A., D. Pantel, Y. Kim, M. Alexe, and D. Hesse. 2013. "Microstructure and Ferroelectric Properties of Epitaxial Cation Ordered $PbSc_{0.5}ta_{0.5}O_3$ Thin Films Grown on Electroded and Buffered Si (100." *Journal of Applied Physics* 114:084107.

Chubachi, Y., K. Sato, and K. Kojima. 1984. "Reflection High Energy Electron Diffraction and X-Ray Studies of AlN Films Grown on Si (111) and Si (001) by Organometallic Chemical Vapour Deposition." *Thin Solid Films* 122:259–70.

Cottone, F., L. Gammaitoni, H. Vocca, M. Ferrari, and V. Ferrari. 2012. "Piezoelectric Buckled Beams for Random Vibration Energy Harvesting." *Smart Materials and Structures* 21:035021.

Defosseux, M., M. Allain, E. Defay, and S. Basrour. 2012. "Highly Efficient Piezoelectric Micro Harvester for Low Level of Acceleration Fabricated with a CMOS Compatible Process." *Sensors and Actuators A: Physical* 188:489–94.

Deterre, M., E. Lefeuvre, Y. Zhu, M. Woytasik, A. Bosseboeuf, B. Boutaud, and R. Dal Molin. 2013. "Micromachined Piezoelectric Spirals and Ultra-Compliant Packaging for Blood Pressure Energy Harvesters Powering Medical Implants." Paper Presented at the IEEE 26th International Conference on Micro Electro Mechanical Systems (MEMS), 249–52.

Dini, M., A. Romani, M. Filippi, and M. Tartagni. 2016. "A Nanopower Synchronous Charge Extractor IC for Low-Voltage Piezoelectric Energy Harvesting with Residual Charge Inversion." *IEEE Transactions on Power Electronics* 31:1263–74.

Du, X.-h, J. Zheng, U. Belegundu, and K. Uchino. 1998. "Crystal Orientation Dependence of Piezoelectric Properties of Lead Zirconate Titanate Near the Morphotropic Phase Boundary." *Applied Physics Letters* 72:2421–3.

Dubois, M.-A., and P. Muralt. 2001. "Stress and Piezoelectric Properties of Aluminum Nitride Thin Films Deposited Onto Metal Electrodes by Pulsed Direct Current Reactive Sputtering." *Journal of Applied Physics* 89:6389–95.

Duffy, M., C. Wang, G. O'clock, S. McFarlane, and P. Zanzucchi. 1973. "Epitaxial Growth and Piezoelectric Properties of A1N, GaN, and GaAS on Sapphire or Spinel." *Journal of Electronic Materials* 2:359–72.

Durou, H., G. A. Ardila-Rodriguez, A. Ramond, X. Dollat, C. Rossi, and D. Esteve. 2010. "Micromachined Bulk Pzt Piezoelectric Vibration Harvester to Improve Effectiveness Over Low Amplitude and Low Frequency Vibrations." *Proceedings of Power MEMS* 27–30.

Dutoit, N. E., B. L. Wardle, and S.-G. Kim. 2005. "Design Considerations for MEMS-Scale Piezoelectric Mechanical Vibration Energy Harvesters." *Integrated Ferroelectrics* 71:121–60.

Elfrink, R., T. Kamel, M. Goedbloed, S. Matova, D. Hohlfeld, Y. Van Andel, and R. Van Schaijk. 2009a. "Vibration Energy Harvesting with Aluminum Nitride-Based Piezoelectric Devices." *Journal of Micromechanics and Microengineering* 19:094005.

Elfrink, R., V. Pop, D. Hohlfeld, T. Kamel, S. Matova, C. De Nooijer, M. Jambunathan, M. Goedbloed, L. Caballero, and M. Renaud. 2009b. "First Autonomous Wireless Sensor Node Powered by a Vacuum-Packaged Piezoelectric MEMS Energy Harvester." Paper presented at the IEEE International Electron Devices Meeting (IEDM), 1–4.

Elfrink, R., M. Renaud, T. Kamel, C. De Nooijer, M. Jambunathan, M. Goedbloed, D. Hohlfeld, S. Matova, V. Pop, and L. Caballero. 2010. "Vacuum-Packaged Piezoelectric Vibration Energy Harvesters: Damping Contributions and Autonomy for a Wireless Sensor System." *Journal of Micromechanics and Microengineering* 20:104001.

Erturk, A., and D. J. Inman. 2008. "On Mechanical Modeling of Cantilevered Piezoelectric Vibration Energy Harvesters." *Journal of Intelligent Material Systems and Structures* 19:1311–25.

Erturk, A., and D. Inman. 2011. "Broadband Piezoelectric Power Generation on High-Energy Orbits of the Bistable Duffing Oscillator with Electromechanical Coupling." *Journal of Sound and Vibration* 330:2339–53.

Fang, H.-B., J.-Q. Liu, Z.-Y. Xu, L. Dong, L. Wang, D. Chen, B.-C. Cai, and Y. Liu. 2006. "Fabrication and Performance of MEMS-Based Piezoelectric Power Generator for Vibration Energy Harvesting." *Microelectronics Journal* 37:1280–4.

Findeisen, D. 2013. *System Dynamics and Mechanical Vibrations: An Introduction*. Berlin: Springer Science & Business Media.

Funakubo, H., M. Dekkers, A. Sambri, S. Gariglio, I. Shklyarevskiy, and G. Rijnders. 2012. "Epitaxial PZT Films for MEMS Printing Applications." *MRS Bulletin* 37:1030–8.

Gardeniers, J., A. Smith, and C. Cobianu. 1995. "Characterisation of Sol-Gel PZT Films on Pt-Coated Substrates." *Journal of Micromechanics and Microengineering* 5:153.

Gasnier, P., J. Willemin, S. Boisseau, G. Despesse, C. Condemine, G. Gouvernet, *et al*. 2014. "An Autonomous Piezoelectric Energy Harvesting IC Based on a Synchronous Multi-Shot Technique." *IEEE Journal of Solid-State Circuits* 49:1561–70.

Ginsberg, J. H., and J. H. Ginsberg. 2001. *Mechanical and Structural Vibrations: Theory and Applications*. New York: Wiley.

Guyomar, D., A. Badel, E. Lefeuvre, and C. Richard. 2005. "Toward Energy Harvesting Using Active Materials and Conversion Improvement by Nonlinear Processing." *IEEE Transactions on Ultrasonics, Ferroelectrics, and Frequency Control* 52:584–95.

Hajati, A. 2011. "Ultra Wide-Bandwidth Micro Energy Harvester." Ph. D. Dissertation in Massachusetts Institute of Technology.

Hajati, A., and S.-G. Kim. 2011. "Ultra-Wide Bandwidth Piezoelectric Energy Harvesting." *Applied Physics Letters* 99:083105.

Hajati, A., R. Xu, and S.-G. Kim. 2011. "Wide Bandwidth Piezoelectric Micro Energy Harvester Based on Nonlinear Resonance." Paper presented at the PowerMEMS.

Han, G., J. Ryu, W.-H. Yoon, J.-J. Choi, B.-D. Hahn, J.-W. Kim, D.-S. Park, C.-W. Ahn, S. Priya, and D.-Y. Jeong. 2011a. "Stress-Controlled $Pb(Zr_{0.52}ti_{0.48})O_3$ Thick Films by Thermal Expansion Mismatch Between Substrate and $Pb(Zr_{0.52}ti_{0.48})O_3$ Film." *Journal of Applied Physics* 110:124101.

Han, G., J. Ryu, W. H. Yoon, J. J. Choi, B. D. Hahn, and D. S. Park. 2011b. "Effect of Film Thickness on the Piezoelectric Properties of Lead Zirconate Titanate Thick Films Fabricated by Aerosol Deposition." *Journal of the American Ceramic Society* 94:1509–13.

Hashemi, S., M. Sawan, and Y. Savaria. 2012. "A High-Efficiency Low-Voltage CMOS Rectifier for Harvesting Energy in Implantable Devices." *Biomedical Circuits and Systems, IEEE Transactions on* 6:326–35.

Heidrich, N., F. Knöbber, S. Hampl, W. Pletschen, R. E. Sah, V. Cimalla, V. Lebedev, and O. Ambacher. 2011. AlN-Basierte Mikroelektromechanische Strukturen Für Implantate *Paper Presented at Transducers'* 11:1642–4.

Hirasawa, T. H., Y. T.-T. Yen, P. K. Wright, A. P. Pisano, and L. Lin. 2010. "Design and Fabrication of Piezoelectric Aluminum Nitride Corrugated Beam Energy Harvester." Paper presented at PowerMEMS, 211–4.

Hwang, G.-T., V. Annapureddy, J. H. Han, D. J. Joe, C. Baek, D. Y. Park, et al. 2015. "A Reconfigurable Rectified Flexible Energy Harvester via Solid-State Single Crystal Grown PMN–PZT." *Adv Energy Mater* 5:1500051.

Isarakorn, D., D. Briand, P. Janphuang, A. Sambri, S. Gariglio, J. Triscone, F. Guy, J. Reiner, C. Ahn, and N. De Rooij. 2011. "The Realization and Performance of Vibration Energy Harvesting MEMS Devices Based on an Epitaxial Piezoelectric Thin Film." *Smart Materials and Structures* 20:025015.

Jaffe, B. 1971. *Piezoelectric Ceramics*. New York: Academic.

Jeon, Y., R. Sood, J.-H. Jeong, and S.-G. Kim. 2005. "MEMS Power Generator with Transverse Mode Thin Film PZT." *Sensors and Actuators A: Physical* 122:16–22.

Jiang, L., and R. Miles. 1999. "A Passive Damper for the Vibration Modes of the Head Actuator in Hard Disk Drives." *Journal of Sound and Vibration* 220:683–94.

Jo, S.-E., M.-S. Kim, and Y.-J. Kim. 2011. "A Resonant Frequency Switching Scheme of a Cantilever Based on Polyvinylidene Fluoride for Vibration Energy Harvesting." *Smart Materials and Structures* 21:015007.

Jumpertz, L., M. Carras, K. Schires, and F. Grillot. 2014. "Regimes of External Optical Feedback in 5.6 Mm Distributed Feedback Mid-Infrared Quantum Cascade Lasers." *Applied Physics Letters* 105:131112.

Kang, M.-G., W.-S. Jung, C.-Y. Kang, and S.-J. Yoon. 2016. "Recent Progress on PZT Based Piezoelectric Energy Harvesting Technologies." *Actuators* 5:5.

Kanno, I., S. Fujii, T. Kamada, and R. Takayama. 1997. "Piezoelectric Properties of c-Axis Oriented $Pb(Zr,Ti)O_3$ Thin Films." *Applied Physics Letters* 70:1378–80.

Kanno, I., T. Ichida, K. Adachi, H. Kotera, K. Shibata, and T. Mishima. 2012. "Power-Generation Performance of Lead-Free (K, Na)NbO_3 Piezoelectric Thin-Film Energy Harvesters." *Sensors and Actuators A: Physical* 179:132–6.

Kim, H.-U., W.-H. Lee, H. R. Dias, and S. Priya. 2009. "Piezoelectric Microgenerators-Current Status and Challenges." *IEEE Transactions on Ultrasonics, Ferroelectrics, and Frequency Control* 56:1555–68.

Kim, H., S. Priya, H. Stephanou, and K. Uchino. 2007. "Consideration of Impedance Matching Techniques for Efficient Piezoelectric Energy Harvesting." *IEEE Transactions on Ultrasonics, Ferroelectrics, and Frequency Control* 54:1851–9.

Kong, N., T. S. Deyerle IV, and D. S. Ha. 2011. "Universal Power Management IC for Small-Scale Energy Harvesting with Adaptive Impedance Matching." Paper presented at the IEEE Energy Conversion Congress and Exposition (ECCE), 3859–63.

Kong, N., and D. S. Ha. 2012. "Low-Power Design of a Self-Powered Piezoelectric Energy Harvesting System with Maximum Power Point Tracking." *IEEE Transactions on Power Electronics* 27:2298–308.

Kong, N., D. S. Ha, A. Erturk, and D. J. Inman. 2010. "Resistive Impedance Matching Circuit for Piezoelectric Energy Harvesting." *Journal of Intelligent Material Systems and Structures* 31:1293–302.

Krulevitch, P., A. P. Lee, P. B. Ramsey, J. C. Trevino, J. Hamilton, and M. A. Northrup. 1996. "Thin Film Shape Memory Alloy Microactuators." *Journal of Microelectromechanical Systems* 5:270–82.

Kuwata, J., K. Uchino, and S. Nomura. 1982. "Dielectric and Piezoelectric Properties of $0.91pb(Zn_{1/3}nb_{2/3})O_3$-$0.09PbTiO_3$ Single Crystals." *Japanese Journal of Applied Physics* 21:1298.

Lam, Y.-H., W.-H. Ki, and C.-Y. Tsui. 2006. "Integrated Low-Loss CMOS Active Rectifier for Wirelessly Powered Devices." *IEEE Transactions on Circuits and Systems II: Express Briefs* 53:1378–82.

Le, T. T., J. Han, A. Von Jouanne, K. Mayaram, and T. S. Fiez. 2006. "Piezoelectric Micro-Power Generation Interface Circuits." *IEEE Journal of Solid-State Circuits* 41:1411–20.

Ledermann, N., P. Muralt, J. Baborowski, S. Gentil, K. Mukati, M. Cantoni, A. Seifert, and N. Setter. 2003. "{1 0 0}-Textured, Piezoelectric $Pb(Zr_x, Ti_{1-x})O_3$ Thin Films for MEMS: Integration, Deposition and Properties." *Sensors and Actuators A: Physical* 105:162–70.

Lee, B., S. Lin, W. Wu, X. Wang, P. Chang, and C. Lee. 2009. "Piezoelectric MEMS Generators Fabricated with an Aerosol Deposition PZT Thin Film." *Journal of Micromechanics and Microengineering* 19:065014.

Lefeuvre, E., A. Badel, C. Richard, and D. Guyomar. 2005. "Piezoelectric Energy Harvesting Device Optimization by Synchronous Electric Charge Extraction." *Journal of Intelligent Material Systems and Structures* 16:865–76.

Lefeuvre, E., S. Risquez, J. Wei, M. Woytasik, and F. Parrain. 2014. "Self-Biased Inductor-Less Interface Circuit for Electret-Free Electrostatic Energy Harvesters." *Journal of Physics: Conference Series, PowerMEMS* 557:012052.

Lefki, K., and G. Dormans. 1994. "Measurement of Piezoelectric Coefficients of Ferroelectric Thin Films." *Journal of Applied Physics* 76:1764–7.

Lei, A., R. Xu, A. Thyssen, A. C. Stoot, T. L. Christiansen, K. Hansen, R. Lou-Moller, E. V. Thomsen, and K. Birkelund. 2011. "MEMS-based Thick Film PZT Vibrational Energy Harvester." Paper presented at the IEEE International Conference on Micro Electro Mechanical Systems (MEMS), 125–8.

Li, J., J. Slutsker, J. Ouyang, and A. Roytburd. 2004. "Contribution of Substrate to Converse Piezoelectric Response of Constrained Thin Films." *Journal of Materials Research* 19:2853–8.

Li, X., and T. Tansley. 1990. "Laser-Induced Chemical Vapor Deposition of AlN Films." *Journal of Applied Physics* 68: 5369–71.

Liu, H., C. Lee, T. Kobayashi, C. J. Tay, and C. Quan. 2012. "Piezoelectric MEMS-Based Wideband Energy Harvesting Systems Using a Frequency-up-Conversion Cantilever Stopper." *Sensors and Actuators A: Physical* 186:242–8.

Lu, C., C.-Y. Tsui, and W.-H. Ki. 2011. "Vibration Energy Scavenging System with Maximum Power Tracking for Micropower Applications." *IEEE Transactions Very Large Scale Integrated VLSI System* 19:2109–19.

Mann, B., and N. Sims. 2009. "Energy Harvesting From the Nonlinear Oscillations of Magnetic Levitation." *Journal of Sound and Vibration* 319:515–30.

Mansour, M. O., M. H. Arafa, and S. M. Megahed. 2010. "Resonator with Magnetically Adjustable Natural Frequency for Vibration

Energy Harvesting." *Sensors and Actuators A: Physical* 163:297–303.
Marin, A. 2013. "Mechanical Energy Harvesting for Powering Distributed Sensors and Recharging Storage Systems." Ph. D. Dissertation in Virginia Tech.
Marin, A., S. Bressers, and S. Priya. 2011. "Multiple Cell Configuration Electromagnetic Vibration Energy Harvester." *Journal of Physics D: Applied Physics* 44:295501.
Marin, A., and S. Priya. 2012. "Multi-Mechanism Vibration Harvester Combining Inductive and Piezoelectric Mechanisms." Paper presented at the SPIE Smart Structures and Materials + Nondestructive Evaluation and Health Monitoring, 83411L-L–11.
Marinkovic, B., and H. Koser. 2009. "Smart Sand-a Wide Bandwidth Vibration Energy Harvesting Platform." *Applied Physics Letters* 94:103505.
Martin, F., P. Muralt, M.-A. Dubois, and A. Pezous. 2004. "Thickness Dependence of the Properties of Highly c-Axis Textured AlN Thin Films." *Journal of Vacuum Science & Technology A* 22:361–5.
Marzencki, M., Y. Ammar, and S. Basrour. 2007. "Design, Fabrication and Characterization of a Piezoelectric MEMS, Vibration Energy Scavenging." Paper presented at the Symposium on Design, Test, Integration and Packaging of MEMS/MOEMS (DTIP'07), 350–3.
Massaro, A., S. De Guido, I. Ingrosso, R. Cingolani, M. De Vittorio, M. Cori, A. Bertacchini, L. Larcher, and A. Passaseo. 2011. "Freestanding Piezoelectric Rings for High Efficiency Energy Harvesting at Low Frequency." *Applied Physics Letters* 98:053502.
Meng, W., J. Heremans, and Y. Cheng. 1991. "Epitaxial Growth of Aluminum Nitride on Si (111) by Reactive Sputtering." *Applied Physics Letters* 59:2097–9.
Miller, L. M., E. Halvorsen, T. Dong, and P. K. Wright. 2011. "Modeling and Experimental Verification of Low-Frequency MEMS Energy Harvesting From Ambient Vibrations." *Journal of Micromechanics and Microengineering* 21:045029.
Mitcheson, P. D., E. K. Reilly, T. Toh, P. K. Wright, and E. M. Yeatman. 2007. "Performance Limits of the Three MEMS Inertial Energy Generator Transduction Types." *Journal of Micromechanics and Microengineering* 17:S211.
Morimoto, K., I. Kanno, K. Wasa, and H. Kotera. 2010. "High-Efficiency Piezoelectric Energy Harvesters of c-Axis-Oriented Epitaxial PZT Films Transferred Onto Stainless Steel Cantilevers." *Sensors and Actuators A: Physical* 163:428–32.
Muralt, P., M. Marzencki, B. Belgacem, F. Calame, and S. Basrour. 2009a. "Vibration Energy Harvesting with PZT Micro Device." *Procedia Chemistry* 1:1191–4.
Muralt, P., R. Polcawich, and S. Trolier-McKinstry. 2009b. "Piezoelectric Thin Films for Sensors, Actuators, and Energy Harvesting." *MRS Bulletin* 34:658–64.
Norton, M. G., P. G. Kotula, and C. B. Carter. 1991. "Oriented Aluminum Nitride Thin Films Deposited by Pulsed-Laser Ablation." *Journal of Applied Physics* 70:2871–3.
Park, J. C., J. Y. Park, and Y.-P. Lee. 2010. "Modeling and Characterization of Piezoelectric-Mode MEMS Energy Harvester." *Journal of Microelectromechanical Systems* 19:1215–22.
Park, S., and T. R. Shrout. 1997. "Ultrahigh Strain and Piezoelectric Behavior in Relaxor Based Ferroelectric Single Crystals." *Journal of Applied Physics* 82:1804–11.
Potrepka, D. M., G. R. Fox, L. M. Sanchez, and R. G. Polcawich. 2011. "Pt/TiO_2 Growth Templates for Enhanced PZT Films and MEMS Devices." Paper presented at the MRS, 67–72.
Priya, S. 2007. "Advances in Energy Harvesting Using Low Profile Piezoelectric Transducers." *Journal of Electroceramics* 19: 167–84.
Priya, S. 2010. "Criterion for Material Selection in Design of Bulk Piezoelectric Energy Harvesters." *IEEE Transactions on Ultrasonics, Ferroelectrics, and Frequency Control* 57: 2610–12.
Priya, S., and D. J. Inman. 2009. "Energy harvesting technologies" Springer.
Qi, Y., J. Kim, T. D. Nguyen, B. Lisko, P. K. Purohit, and M. C. McAlpine. 2011. "Enhanced Piezoelectricity and Stretchability in Energy Harvesting Devices Fabricated From Buckled PZT Ribbons." *Nano Letters* 11:1331–6.
Ramadass, Y. K., and A. P. Chandrakasan. 2010. "An Efficient Piezoelectric Energy Harvesting Interface Circuit Using a Bias-Flip Rectifier and Shared Inductor." *IEEE Journal of Solid-State Circuits* 45:189–204.
Reilly, E. K., L. M. Miller, R. Fain, and P. Wright. 2009. "A Study of Ambient Vibrations for Piezoelectric Energy Conversion." *Proc. PowerMEMS* 2009:312–15.
Renaud, M., K. Karakaya, T. Sterken, P. Fiorini, C. Van Hoof, and R. Puers. 2008. "Fabrication, Modelling and Characterization of MEMS Piezoelectric Vibration Harvesters." *Sensors and Actuators A: Physical* 145:380–6.
Rincón-Mora, G. A., and S. Yang. 2016. "Tiny Piezoelectric Harvesters: Principles, Constraints, and Power Conversion." *IEEE Trans on Circuits and Systems I: Regular Papers* 63: 639–49.
Roundy, S., and P. K. Wright. 2004. "A Piezoelectric Vibration Based Generator for Wireless Electronics." *Smart Materials and Structures* 13:1131.
Roundy, S., P. K. Wright, and J. Rabaey. 2003a. "A Study of Low Level Vibrations as a Power Source for Wireless Sensor Nodes." *Computer Communications* 26:1131–44.
Roundy, S., P. K. Wright, and J. Rabaey. 2003b. *Energy Scavenging for Wireless Sensor Networks*. Kluwer Academic Publishers.
Ryu, J., J.-J. Choi, B.-D. Hahn, D.-S. Park, W.-H. Yoon, and K.-H. Kim. 2007. "Fabrication and Ferroelectric Properties of Highly Dense Lead-Free Piezoelectric ($K_{0.5}na_{0.5}$) NbO_3 Thick Films by Aerosol Deposition." *Appl. Phys. Lett* 90:152901.
Ryu, J., G. Han, T. K. Song, A. Welsh, S. Trolier-McKinstry, H. Choi, J.-P. Lee, J.-W. Kim, W.-H. Yoon, and J.-J. Choi. 2014. "Upshift of Phase Transition Temperature in Nanostructured $PbTiO_3$ Thick Film for High Temperature Applications." *ACS Applied Materials & Interfaces* 6:11980–7.
Saggini, S., S. Giro, F. Ongaro, and P. Mattavelli. 2010. "Implementation of Reactive and Resistive Load Matching for Optimal Energy Harvesting from Piezoelectric Generators." Paper presented at the IEEE Workshop on Control and Modeling for Power Electronics (COMPEL), 1–6.
Sanchez, L. M., D. M. Potrepka, G. R. Fox, I. Takeuchi, K. Wang, L. A. Bendersky, and R. G. Polcawich. 2013. "Optimization of $PbTiO_3$ Seed Layers and Pt Metallization for PZT-Based piezoMEMS Actuators." *J. Mater. Res* 28:1920–31.
Sankman, J., and D. Ma. 2014. "A 12-μw to 1.1-mW AIM Piezoelectric Energy Harvester for Time-Varying Vibrations with 450 nA IQ." *IEEE Trans. Power Electron* 30:632–43.

Saxler, A., P. Kung, C. Sun, E. Bigan, and M. Razeghi. 1994. "High Quality Aluminum Nitride Epitaxial Layers Grown on Sapphire Substrates." *Applied Physics Letters* 64:339–41.

Sessler, G. M. 2001. "Electrets: Recent Developments." *Journal of Electrostatics* 51–52:137–45.

Sharpes, N., A. Abdelkefi, and S. Priya. 2015. "Two-Dimensional Concentrated-Stress Low-Frequency Piezoelectric Vibration Energy Harvesters." *Applied Physics Letters* 107:093901.

Shen, D., J.-H. Park, J. Ajitsaria, S.-Y. Choe, H. C. Wikle III, and D.-J. Kim. 2008. "The Design, Fabrication and Evaluation of a MEMS PZT Cantilever with an Integrated Si Proof Mass for Vibration Energy Harvesting." *Journal of Micromechanics and Microengineering* 18:055017.

Shibata, K., K. Suenaga, K. Watanabe, F. Horikiri, A. Nomoto, and T. Mishima. 2011. "Improvement of Piezoelectric Properties of (K, Na)NbO_3 Films Deposited by Sputtering." *Japanese Journal of Applied Physics* 50:041503.

Shim, M., J. Kim, J. Jeong, S. Park, and C. Kim. 2015. "Self-Powered 30 μw to 10 mW Piezoelectric Energy Harvesting System with 9.09 Ms/V Maximum Power Point Tracking Time." *IEEE J. Solid-State Circuits* 50:2367–79.

Shiosaki, T., T. Yamamoto, T. Oda, and A. Kawabata. 1980. "Low-Temperature Growth of Piezoelectric AlN Film by Rf Reactive Planar Magnetron Sputtering." *Applied Physics Letters* 36: 643–5.

Sorimachi, A., H. Takahashi, and S. Tokonami. 2009. "Influence of the Presence of Humidity, Ambient Aerosols and Thoron on the Detection Responses of Electret Radon Monitors." *Radiation Measurements* 44:111–15.

Stevens, K., A. Ohtani, M. Kinniburgh, and R. Beresford. 1994. "Microstructure of AlN on Si (111) Grown by Plasma-Assisted Molecular Beam Epitaxy." *Applied Physics Letters* 65:321–3.

Stoppel, F., C. Schröder, F. Senger, B. Wagner, and W. Benecke. 2011. "AlN-Based Piezoelectric Micropower Generator for Low Ambient Vibration Energy Harvesting." *Procedia Engineering* 25:721–4.

Tabesh, A., and L. G. Fréchette. 2010. "A Low-Power Stand-Alone Adaptive Circuit for Harvesting Energy From a Piezoelectric Micropower Generator." *Industrial Electronics, IEEE Transactions on* 57:840–9.

Takeda, F., T. Mori, and T. Takahashi. 1981. "Effect of Hydrogen Gas on c-Axis Oriented AlN Films Prepared by Reactive Magnetron Sputtering." *Japanese Journal of Applied Physics* 20:L169.

Ting-Ta, Y., T. Hirasawa, P. Wright, A. Pisano, and L. Liwei. 2011. "Corrugated Aluminum Nitride Energy Harvesters for High Energy Conversion 26. Effectiveness." *J. Micromech. Microeng* 21:085037.

Trolier-McKinstry, S., and P. Muralt. 2004. "Thin Film Piezoelectrics for MEMS." *Journal of Electroceramics* 12:7–17.

Tsubouchi, K., and N. Mikoshiba. 1985. "Zero-Temperature-Coefficients SAW Devices on AlN Epitaxial Films." *IEEE Transactions on Sonics and Ultrasonics* 32:634–44.

Tsujiura, Y., E. Suwa, H. Hida, K. Suenaga, K. Shibata, and I. Kanno. 2013. "Lead-Free Piezoelectric MEMS Energy Harvesters of Stainless Steel Cantilevers." Paper Presented at the Transducers & Eurosensors XXVII: The 17th International Conference on Solid-State Sensors, Actuators and Microsystems, 474–7.

Tuttle, B., J. A. Voigt, T. J. Garino, D. C. Goodnow, R. W. Schwartz, D. L. Lamppa, T. J. Headley, and M. O. Eatough. 1992. "Chemically Prepared Pb(Zr,Ti)O_3 Thin Films: The Effects of Orientation and Stress." Paper presented at the IEEE International Symposium on Applications of Ferroelectrics, 344–8.

Uchino, K. 2009. *Ferroelectric Devices*, 2nd ed. CRC press.

Van Schaijk, R., R. Elfrink, T. Kamel, and M. Goedbloed. 2008. "Piezoelectric AlN Energy Harvesters for Wireless Autonomous Transducer Solutions." Paper presented at the IEEE Sensors, 45–8.

Varghese, R. P. 2013. "MEMS Technologies for Energy Harvesting and Sensing." Ph. D. Disseration in Virginia Tech.

Varghese, R., M. Williams, S. Gupta, and S. Priya. 2011. "Temperature-Time Transformation Diagram for Pb(Zr, Ti)O_3 Thin Films." *Journal of Applied Physics* 110:014109.

Wang, Q.-M., X.-H. Du, B. Xu, and L. E. Cross. 1999. "Electromechanical Coupling and Output Efficiency of Piezoelectric Bending Actuators." *IEEE Transactions on Ultrasonics, Ferroelectrics, and Frequency Control* 46: 638–46.

Wang, X.-Y., C.-Y. Lee, Y.-C. Hu, W.-P. Shih, C.-C. Lee, J.-T. Huang, and P.-Z. Chang. 2008. "The Fabrication of Silicon-Based PZT Microstructures Using an Aerosol Deposition Method." *Journal of Micromechanics and Microengineering* 18:055034.

Wang, Z. L., and J. Song. 2006. "Piezoelectric Nanogenerators Based on Zinc Oxide Nanowire Arrays." *Science* 312:242–6.

Wu, L., X.-D. Do, S.-G. Lee, and D. S. Ha, A Self-Powered and Optimal SSHI Circuit Integrated with an Active Rectifier for Piezoelectric Energy Harvesting to appear in IEEE Trans. on Circuits and Systems I.

Xu, R. 2012. "The Design of Low-Frequency, Low-G Piezoelectric Micro Energy Harvesters." *Ph. D. Dissertation in Massachusetts Institute of Technology*.

Xu, R., and S. Kim. 2012. "Figures of Merits of Piezoelectric Materials in Energy Harvesters." Paper presented at the Power MEMS.

Xu, R., and S. Kim. 2015. "Low-Frequency, Low-G MEMS Piezoelectric Energy Harvester." Paper presented at the Power MEMS, 012013.

Xu, R., A. Lei, C. Dahl-Petersen, K. Hansen, M. Guizzetti, K. Birkelund, E. V. Thomsen, and O. Hansen. 2012a. "Fabrication and Characterization of MEMS-Based PZT/PZT Bimorph Thick Film Vibration Energy Harvesters." *Journal of Micromechanics and Microengineering* 22:094007.

Xu, R., A. Lei, C. Dahl-Petersen, K. Hansen, M. Guizzetti, K. Birkelund, E. V. Thomsen, and O. Hansen. 2012b. "Screen Printed PZT/PZT Thick Film Bimorph MEMS Cantilever Device for Vibration Energy Harvesting." *Sensors and Actuators A: Physical* 188:383–8.

Yen, T.-T., T. Hirasawa, P. K. Wright, A. P. Pisano, and L. Lin. 2011. "Corrugated Aluminum Nitride Energy Harvesters for High Energy Conversion Effectiveness." *Journal of Micromechanics and Microengineering* 21:085037.

Yeo, H. G., and S. Trolier-McKinstry. 2014. "{001} Oriented Piezoelectric Films Prepared by Chemical Solution Deposition on Ni Foils." *Journal of Applied Physics* 116:014105.

Yokoyama, S., T. Ozeki, T. Oikawa, and H. Funakubo. 2002. "Preparation of Orientation-Controlled Polycrystalline Pb(Zr, Ti)O_3 Thick Films on (100) Si Substrates by Metalorganic Chemical Vapor Deposition and Their Electrical Properties." *Japanese Journal of Applied Physics* 41:6705.

Zhang, W., Y. Someno, M. Sasaki, and T. Hirai. 1993. "Low-Temperature Epitaxial Growth of AlN Films on Sapphire by

Electron Cyclotron Resonance Plasma-Assisted Chemical Vapor Deposition." *Journal of Crystal Growth* 130:308–12.

Zhou, Y., D. J. Apo, and S. Priya. 2013a. "Dual-Phase Self-Biased Magnetoelectric Energy Harvester." *Applied Physics Letters* 103:192909.

Zhou, Q., S. Lau, D. Wu, and K. K. Shung. 2011. "Piezoelectric Films for High Frequency Ultrasonic Transducers in Biomedical Applications." *Progress in Materials Science* 56:139–74.

Zhou, Y., C.-S. Park, C.-H. Wu, D. Maurya, M. Murayama, A. Kumar, R. Katiyar, and S. Priya. 2013b. "Microstructure and Surface Morphology Evolution of Pulsed Laser Deposited Piezoelectric $BaTiO_3$ Films." *Journal of Materials Chemistry C* 1:6308–15.

Zhu, D., S. Roberts, J. Tudor, and S. Beeby. 2008. "Closed Loop Frequency Tuning of a Vibration-based Micro-Generator." Paper presented at the Power MEMS, 229–32.